

AD-A191 219

DTIC FILE COPY

2



AFWAL-TR-87-3059

STRESS INTENSITY FACTORS FOR CRACKED METALLIC STRUCTURES UNDER RAPID  
THERMAL LOADING

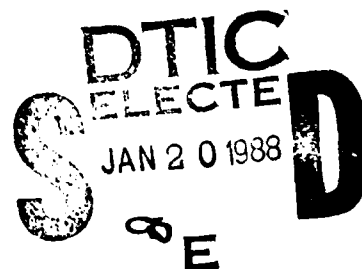
Russell C. Cipolla  
Kimble J. Clark

Aptech Engineering Services, Inc.  
Sunnyvale, California 94089

October 1987

Final Report for Period August 1986 - May 1987

Approved for public release; distribution unlimited.



FLIGHT DYNAMICS LABORATORY  
AIR FORCE WRIGHT AERONAUTICAL LABORATORIES  
AIR FORCE SYSTEMS COMMAND  
WRIGHT-PATTERSON AIR FORCE BASE, OHIO 45433-6553

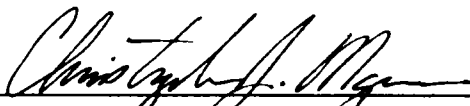
88 1 15 020

## NOTICE

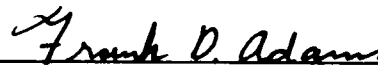
When Government drawings, specifications, or other data are used for any purpose other than in connection with a definitely Government-related procurement, the United States Government incurs no responsibility or any obligation whatsoever. The fact that the Government may have formulated or in any way supplied the said drawings, specifications, or other data, is not to be regarded by implication, or otherwise in any manner construed, as licensing the holder, or any other person or corporation; or as conveying any rights or permission to manufacture, use, or sell any patented invention that may in any way be related thereto.

This report has been reviewed by the Office of Public Affairs (ASD/PA) and is releasable to the National Technical Information Service (NTIS). At NTIS, it will be available to the general public, including foreign nations.

This technical report has been reviewed and is approved for publication.

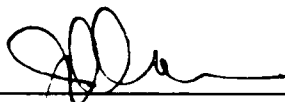


CHRISTOPHER D. MAZUR, Capt., USAF  
Fatigue, Fracture & Reliability Group  
Structural Integrity Branch



FRANK D. ADAMS, Chief  
Structural Integrity Branch  
Structures Division

FOR THE COMMANDER



JAMES J. OLSEN  
Acting Chief  
Structures Division

If your address has changed, if you wish to be removed from our mailing list, or if the addressee is no longer employed by your organization, please notify AFWAL/FIBEC, Wright-Patterson AFB, OH 45433-6553 to help us maintain a current mailing list.

Copies of this report should not be returned unless return is required by security considerations, contractual obligations, or notice on a specific document.

UNCLASSIFIED

SECURITY CLASSIFICATION OF THIS PAGE

REPORT DOCUMENTATION PAGE				Form Approved OMB No. 0704-0188	
1a. REPORT SECURITY CLASSIFICATION UNCLASSIFIED			1b. RESTRICTIVE MARKINGS		
2a. SECURITY CLASSIFICATION AUTHORITY			3. DISTRIBUTION / AVAILABILITY OF REPORT Approved for public release; distribution unlimited		
2b. DECLASSIFICATION / DOWNGRADING SCHEDULE					
4. PERFORMING ORGANIZATION REPORT NUMBER(S) AES-8609709F-1			5. MONITORING ORGANIZATION REPORT NUMBER(S) AFWAL-TR-87-3059		
6a. NAME OF PERFORMING ORGANIZATION APTECH Engineering Services		6b. OFFICE SYMBOL (If applicable)	7a. NAME OF MONITORING ORGANIZATION Flight Dynamics Laboratory (AFWAL/FIBEC) Air Force Wright Aeronautical Laboratories		
6c. ADDRESS (City, State, and ZIP Code) 1257 Elko Drive Sunnyvale CA 94089			7b. ADDRESS (City, State, and ZIP Code) Wright-Patterson AFB, OH 45433-6553		
8a. NAME OF FUNDING / SPONSORING ORGANIZATION DOD SBIR Program Office		8b. OFFICE SYMBOL (If applicable)	9. PROCUREMENT INSTRUMENT IDENTIFICATION NUMBER F33615-86-C-3217		
8c. ADDRESS (City, State, and ZIP Code) Washington DC 20301			10. SOURCE OF FUNDING NUMBERS		
			PROGRAM ELEMENT NO. 65502F	PROJECT NO. 3005	TASK NO. 30
11. TITLE (Include Security Classification) Stress Intensity Factors for Cracked Metallic Structures under Rapid Thermal Loading					
12. PERSONAL AUTHOR(S) Russell C. Cipolla, Kimble J. Clark					
13a. TYPE OF REPORT Final		13b. TIME COVERED FROM 0886 TO 0587		14. DATE OF REPORT (Year, Month, Day) 1987, October	
15. PAGE COUNT 68					
16. SUPPLEMENTARY NOTATION This is a small business Innovative Research Program, PHASE I Report					
17. COSATI CODES			18. SUBJECT TERMS (Continue on reverse if necessary and identify by block number) Stress Intensity Factors, Fracture Mechanics, Rapid Thermal Pulses, Crack Growth, Analysis		
FIELD	GROUP	SUB-GROUP			
13	13				
20	05				
19. ABSTRACT (Continue on reverse if necessary and identify by block number) High intensity heating of aircraft structures can challenge the structural integrity of critical aircraft components, especially when they may contain flaws. The evaluation of flawed components requires the application of fracture mechanics wherein crack tip stress intensity factors are used to provide a quantitative means of assessing structural integrity. The primary objectives of this project were to develop an analysis method for computing stress intensity factors for severe thermal loadings of interest to the Air Force and to demonstrate the applicability of the method to small microcomputers.  A methodology was developed based on influence functions to determine stress intensity factors for structures exposed to intense thermal heating. As a demonstration of the methodology, the calculation of stress intensity factors (K) for a flaw in a flat plate was performed for two surface heating problems--laser beam impingement and aerodynamic					
20. DISTRIBUTION / AVAILABILITY OF ABSTRACT <input type="checkbox"/> UNCLASSIFIED/UNLIMITED <input type="checkbox"/> SAME AS RPT <input checked="" type="checkbox"/> DTIC USERS			21. ABSTRACT SECURITY CLASSIFICATION UNCLASSIFIED		
22a. NAME OF RESPONSIBLE INDIVIDUAL Capt Christopher Mazur			22b. TELEPHONE (Include Area Code) (513) 255-6104		22c. OFFICE SYMBOL AFWAL/FIBEC

# 19. Abstract (con't)

heating. A solution algorithm was developed based on the influence function method, and numerical results were generated to show the variation of K with flaw size and orientation as well as relevant thermal parameters involving surface heat flux and heat duration. These results suggest that the contribution to the crack driving force by localized severe heating is significant and can exceed 20 percent of the static fracture toughness of the material.

The numerical algorithms developed can be executed on a desktop microcomputer illustrating the efficient and powerful characteristic of the influence function method to solve highly complex cracked body problems. A comparison between different 16-bit microprocessor systems and an IBM-3081 mainframe show competitive execution performance with no expected loss in solution accuracy. Potential applications for this methodology include useful engineering workstation software for damage tolerance design as well as on board expert systems for monitoring structural integrity during flight and mission performance.

Accession For	
NTIS GRA&I	<input checked="" type="checkbox"/>
DTIC TAB	<input type="checkbox"/>
Unannounced	<input type="checkbox"/>
Justification	
By	
Distribution/	
Availability Codes	
Dist	Avail and/or Special
A-1	



## TABLE OF CONTENTS

<u>Section</u>	<u>Page</u>
1 INTRODUCTION	1-1
Background	1-1
Project Scope	1-2
2 STRATEGY AND OBJECTIVES	2-1
3 DETERMINATION OF STRESS INTENSITY FACTORS	3-1
Fracture Mechanics Concepts	3-1
Introduction	3-1
Linear Elastic Fracture Mechanics Principles	3-3
Analysis Methodology	3-5
Introduction	3-5
Influence Function Method	3-6
Superposition and Crack Face Loading Equivalence	3-7
Influence Function Generation	3-10
Influence Functions For Two Cracked Body Geometries	3-12
Through Cracked Infinite Plate	3-12
Edge Cracked Plate	3-14
Verification of Solutions	3-14
4 THERMAL ANALYSIS MODELS	4-1
Introduction	4-1
Radial Heat Transfer in a Semi-Infinite Plane	4-2
Governing Equations	4-2
Numerical Solution	4-6
Through Thickness Heat Flow in a Curved Shell	4-8
Governing Equations	4-8
Numerical Solution	4-11
Thermal Stress Analysis	4-13
5 LASER BEAM IRRADIATION ON A FLAT PLANE	5-1
Problem Parameters	5-1
Geometry	5-1
Thermal Parameters and Material Properties	5-1
Stress Solutions	5-4
Stress Intensity Factors	5-6
Effect of Aerodynamic Cooling	5-11
6 AERODYNAMIC HEATING OF A PLANE SURFACE	6-1
Problem Parameters	6-1
Stress Solutions	6-2
Stress Intensity Factors	6-2

<u>Section</u>	<u>Page</u>
7	COMPUTER HARDWARE AND SOFTWARE REQUIREMENTS
	Introduction
	Problem Execution
	Software Specification
8	SUMMARY AND CONCLUSIONS
	REFERENCES

## FIGURES

Figure		Page
3-1	Schematic Showing the Relationship Between Failure Stress and Flaw Size For Two Limiting Failure Modes	3-2
3-2	Review of Linear Elastic Fracture Mechanics	3-4
3-3	Cracked Body Subject to Three Different Loadings	3-9
3-4	Through Cracked Infinite Panel of Uniform Thickness	3-13
3-5	Geometry For Edge Cracked Plate	3-15
3-6	Comparison of Numerical Results From Influence Function Method with Theory For the Case of Uniform Tension	3-17
4-1	Schematic of Laser Beam Impingement Area on Exposed Metal Surface	4-3
4-2	Lumped Mass Heat Conduction Model	4-7
4-3	Thermal Model Geometry	4-9
5-1	The Geometry of an Infinite Plane containing a Through Thickness Crack and Subjected to Laser Heating	5-2
5-2	Temperature Distribution For Two Flux Levels at $t = 0.5$ Second	5-5
5-3	Stress Distribution For Two Laser Flux Levels at $t = 0.5$ Second	5-7
5-4	Variation of $K$ with Time During Laser Irradiation	5-8
5-5	Stress Intensity Factor Versus Crack Length for Two Laser Flux Cases After 2 Seconds of Exposure	5-10
5-6	Mode II Stress Intensity Factor for Two Laser Flux Cases After 2 Seconds of Exposure (Note: $K_I \leq 1$ ksi In $^{1/2}$ for the Above 45° Crack)	5-12
5-7	Effect of Aerodynamic Cooling on Stress Intensity Factor	5-13
6-1	Temperature Response of a Slab Aerodynamically Heated on One Side	6-3
6-2	Thermal Stress in a Slab Subjected to Aerodynamic Heating on One Side	6-4
6-3	Stress Intensity Factor Variation with Time	6-5
7-1	Flowchart Showing General Numerical Procedure	7-5

## TABLES

<u>Table</u>		<u>Page</u>
5-1	Summary of Properties of Aluminum Alloy 7075-T6	5-3
7-1	Summary of Computer Hardware Problem Execution Performance (Times in Seconds)	7-3

## Section 1

### INTRODUCTION

#### BACKGROUND

Maintaining structural integrity of thin section aircraft components when they may contain potential flaws is the primary objective of damage tolerance evaluations. Because integrity of aircraft structures may become challenged by severe and rapid heating, especially when the resulting thermal loads are superimposed with the aerodynamic loads of normal flight, accurate damage tolerance analysis must consider the effect of thermal environment on structural reliability (1, 2).

High intensity heating of aircraft structures may be produced by aerodynamic heating, by laser irradiation, or by localized intense fire. Structural reliability will be reduced by the development of thermal stresses as well as the degradation of strength properties at elevated temperatures caused by the heating. The failure modes resulting from these conditions include localized melting or complete burn through. Such conditions could result in brittle or ductile fracture, or buckling of thin sections depending on the nature of the combined stress state and the type, size, and location of existing flaws.

Fully plastic failure of unflawed aluminum panels by plastic collapse has been studied to the extent where analytical predictions of the residual strength are in good agreement with experimental measurements (1). These predictions are based on transient heat transfer analysis of the thermal heating and straightforward stress analysis to determine the failure load from a fracture strength versus temperature relationship. In the investigation performed herein, similar analytical methods for heat flow and stress analysis have been developed to calculate the crack driving force in flawed metallic structures. The emphasis of the methodology will be to establish the conditions for

nonductile crack extension where thermal heating is severe enough to increase tensile loadings in critical structure components where cracking may exist.

#### PROJECT SCOPE

In failure analysis evaluations of flawed structures, the application of fracture mechanics provides a quantitative means of assessing structural integrity. The fracture mechanics approach to structural reliability accepts that flaws will exist and that conditions can be established where flaws will remain stable and not grow to an unacceptable size during service between inspection intervals. Fracture mechanics evaluations require the calculation of crack tip stress intensity factor ( $K$ ) which defines the severity of the flaw in terms of its physical size and the applied stress acting on it. By calculating  $K$  and comparing it with the material fracture toughness, the ability of a given loading condition and flaw dimensions to cause unstable fracture can be studied.

The development of a general methodology for determining stress intensity factors for aircraft structures exposed to intense thermal heating will require a materials property data base at elevated temperatures, a nonlinear heat transfer analysis model, a thermal stress analysis model, and a fracture mechanics solution technique for determining  $K$ . Although the problem is very complex, the present investigation analytically examines the behavior of through-cracked and part-through-cracked aluminum panels subjected to intense heating. Several simplifying assumptions and model idealizations have been made in order to demonstrate the technique in this Phase I project. Stress intensity factors are computed by the influence function method for a range of crack locations within the panel relative to the position of the heat source. The usefulness of the method is demonstrated by both the presentation of numerical results and the illustration of the ability to solve these complex problems on desktop microcomputers.

## Section 2

### STRATEGY AND OBJECTIVES

The strategy employed in this work for calculating stress intensity factors was to use a weight or influence function approach. As will be discussed later, this technique is very efficient and enables the basic method to provide accurate results using small microcomputers without the need for large mainframe computers. Because the influence function method requires as input the distribution of stress in the structure at the location of the postulated flaw, a thermal stress solution method was also developed which can be executed on a small microcomputer.

The primary objectives of this project were:

- To develop an influence function algorithm complete with the thermal stress solution for calculating stress intensity factors
- To demonstrate the method for two simple engineering problems
- To specify the general requirements for a computer program that will run on a desktop microcomputer

Feasibility of this overall approach is shown in Section 5 by successfully demonstrating stress intensity factor calculations for the following two problems: (1) through-cracked panel subject to laser beam impingement in the vicinity of the crack and (2) an edge-cracked plate subjected to aerodynamic heating on one side. Problem input parameters for thermal flux, absorptivity, and heat losses due to convection and radiation were thoroughly researched to provide a meaningful demonstration of the method. Verification of the accuracy of the developed software is shown by comparing stress intensity factor results calculated here with published results for some simple cases.

### Section 3

#### DETERMINATION OF STRESS INTENSITY FACTORS

##### FRACTURE MECHANICS CONCEPTS

###### Introduction

In applying fracture mechanics analysis to failure prevention evaluations, it is important to establish the possible modes by which the structure may fail. Also, the parameters which are important in determining the residual strength of a structure containing defects must be defined. The failure behavior of structural metals can be classified into three regimes. The disciplines required to assess these regimes are:

- Linear elastic fracture mechanics (LEFM) - The structure fails in a brittle manner, and on a macroscale, the load to failure occurs within nominally elastic loading.
- Elastic-plastic fracture mechanics (EPFM) - The structure fails in a ductile manner, and significant stable crack extension by tearing may precede ultimate failure.
- Limit load or plastic collapse - The failure event is characterized by local large deflections and local plastic strains associated with ultimate strength collapse at a cross section (the structure exhausts its redundancy through the development of multiple local plastic instabilities until, under continued application of load, global collapse occurs).

A schematic diagram showing the relationship between critical or failure stress (i.e., residual structural strength) and flaw size is shown in Figure 3-1 for the failure modes previously described. The shape and position

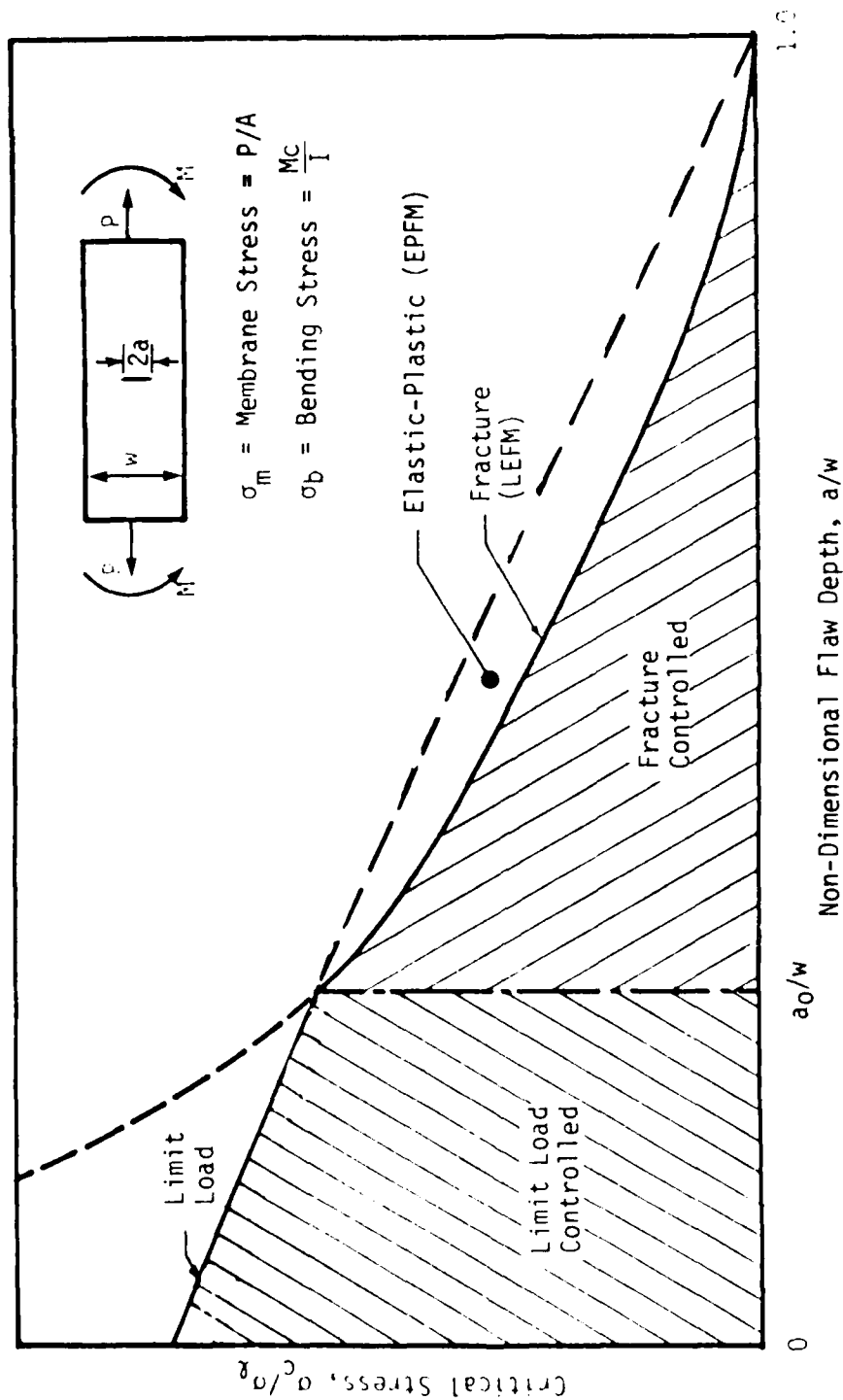


Figure 3-1 - Schematic Showing the Relationship Between Failure Stress and Flaw Size For Two Limiting Failure Modes.

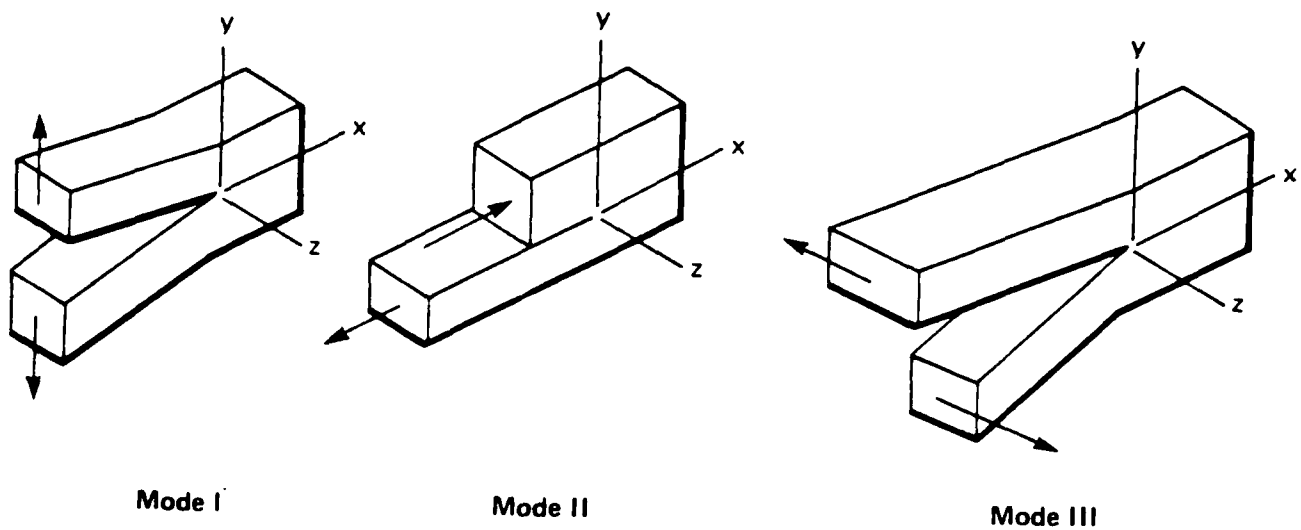
of the failure locus will depend on the fracture toughness ( $K_{Ic}$ ) and strength properties ( $\sigma_{uts}$ ) of the material as well as the structural geometry and type of loading.

Linear elastic fracture mechanics is used most appropriately to describe the behavior of low toughness/high strength materials in which the plastic zone is small relative to the structural geometry and little ductility precedes fracture. With this method, no account is taken of increased material resistance to brittle failure when significant plasticity occurs. For thermal stress problems considered in this application, it is assumed that flaws are primarily driven by thermal loads that will elevate stresses local to the flaw by the elastic constraint to thermal displacements. Hence, flaws located in the vicinity of rapid thermal change will behave elastically provided that the thermal stresses are nominally low (below material yield strength). For this condition, LEFM theory will apply and we restrict our discussion to this case.

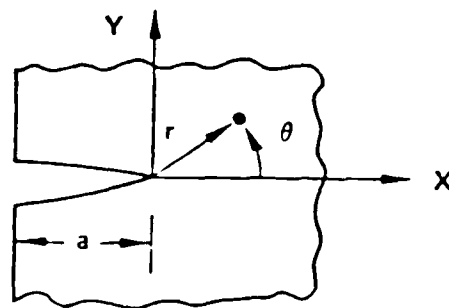
#### Linear Elastic Fracture Mechanics Principles

The principles of LEFM effectively link three parameters--the flaw size, the fracture toughness of the material, and the applied stress. If any two of these are known, the critical value of the third can be quantified. Although the stress distribution of a cracked structure for an arbitrary mode of loading and shape of body and crack can be quite difficult to determine, only three deformation modes can occur near the tip of the crack; the faces can be pulled apart (Mode I) or sheared perpendicular or parallel to the leading edge of the crack (Modes II or III). These three loading modes are shown schematically in Figure 3-2a and the character of the crack near-tip stress distribution is illustrated in Figure 3-2b. The crack opening mode or Mode I in which the load is applied normal to the crack face is generally considered the most damaging of the three modes.

As mentioned above, the most useful parameter for describing the character of the crack near-tip stress distribution is the stress intensity factor. The stress intensity factor ( $K$ ) defines the local crack tip response to global



(a) Basic Crack Opening Modes.



All stress components have the form:

$$\sigma_{ij} = \frac{K_k}{\sqrt{2\pi r}} f_{ij}^{(k)}(\theta)$$

Where  $i = x, y, z$ ;  $j = x, y, z$ ; and  $k = I, II, III$

(b) Near Tip Stress Components.

Figure 3-2 - Review of Linear Elastic Fracture Mechanics.

conditions and is calculated in terms of the nominally applied stress ( $\sigma$ ), the crack length ( $a$ ), and a factor that depends on the flaw geometry, stress distribution, and structural displacement constraints ( $F(a)$ ) from the relation:

$$K = F\sigma\sqrt{\pi a} \quad (3-1)$$

Assuming Mode I loading, fracture is predicted when the applied  $K_I$  value reaches a critical level. For plane strain conditions, this critical level is the fracture toughness,  $K_{Ic}$ , and a requirement for safe service is:

$$K_I < K_{Ic} \quad (3-2)$$

The critical value of applied stress can be computed in terms of flaw size and fracture toughness from the expression:

$$\sigma_c = \frac{K_{Ic}}{F\sqrt{\pi a}} \quad (3-3)$$

Likewise, given the applied stress and critical toughness, the critical flaw size can be determined implicitly from:

$$a_c = \frac{1}{\pi} \left( \frac{K_{Ic}}{\sigma F} \right)^2 \quad (3-4)$$

A detailed discussion on the computation of  $K_I$  follows next.

## ANALYSIS METHODOLOGY

### Introduction

Although many closed form or approximate solutions exist for  $K$ , often numerical techniques are required to calculate  $K$  accurately for the actual structure. A numerical approach was required for the thermal problems considered herein because of the complex stress state expected for the thermal behavior of metal structures subjected to rapid thermal heating. Examination

of Eq. (3-1) shows that the key element in calculating  $K$  is the determination of the function  $F(a)$ , which carries all the information concerning the influence of load distribution and geometry. Clearly, if  $K$  has been computed as a function of  $\sigma$  and  $a$ , then the desired nondimensional function  $F(a)$  is determined trivially.

Traditional numerical methods for calculating  $K$  are either energy based or crack tip stress/displacement based techniques. These stress analysis methods involve the direct modelling of crack face boundaries with very refined regions of discrete elements or nodes in the stress solution. Such traditional approaches will not be applicable for use with microcomputers because of the significant numerical effort required. Under certain circumstances, solution of the stress intensity factor for one set of loadings on a solid provides sufficient information to generate easily stress intensity factor solutions for a complete class of loadings. This approach is known as the influence function method, and its highly efficient nature is exploited in this investigation. This characteristic not only provides accurate  $K$  solutions for thermal problems but also allows the method to be used on small computers.

#### Influence Function Method

The influence function method is a numerical technique that allows for the calculation of  $K$  for nonlinear (general) varying stress distribution acting on the crack. The influence function or weight method was developed by Bueckner (3) and clarified later by Rice (4) for two-dimensional problems. The approach was expanded to three-dimensional problems by Besuner (5) and Cruse (6). Results developed by Bueckner in 1958 (7) are of considerable value for application to problems dealing with body forces, thermal effects, and residual stress.

The influence function ( $h$ ) is a function of crack position ( $x$ ), specified displacement boundary conditions ( $u$ ), and geometry. The calculation of  $K$  for the general class of crack problems in Mode I is:

$$K = \int_L h(x)\sigma(x)dx \quad (3-5)$$

where  $L$  is the crack line and  $\sigma(x)$  is the "uncracked" stress distribution normal to the crack face. Once the influence function has been formulated for a given crack configuration, the stress intensity factor for any applied stress field determined from the uncracked geometry can be computed by simple numerical integration of Eq. (3-5).

The essential features in the formulation of the influence function method are based on the following fundamentals:

- The application of elastic superposition allows the use of the uncracked stress distributions in the  $K$  analysis.
- The influence function itself is invariant with stress and provides the vehicle to calculate the effect of the crack in redistributing any stress field.

The background and basis of the above principles and their impact on simplifying the computational effort are described in the next two subsections.

#### Superposition and Crack Face Loading Equivalence

The principle of superposition reduces the  $K$  solution of an arbitrary and perhaps difficult crack problem to two simpler problems--the stress analysis problem but without the crack and the problem of a cracked body with an applied pressure that cancels the uncracked stress field to establish the traction free boundary conditions along the crack face.

In Bueckner's formulation, he applies the theorems of Clapeyron and Betti to demonstrate that  $K$  for an arbitrary cracked body subject to remotely applied stresses, displacements, and body forces is identical to that due to a simple loading system on the crack face (7, 8). This principle is illustrated in Figure 3-3. The general cracked body problem shown in Figure 3-3a is considered to be the sum of two other problems shown in Figures 3-3b and 3-3c. Hence:

$$K^{(a)} = K^{(b)} + K^{(c)}$$

In the original problem (Figure 3-3a), the cracked body is subject to loading involving surface tractions over Boundary  $S_1$ , imposed displacements over Boundary  $S_2$ , and body forces within the volume ( $V$ ) of the body. A stress free crack exists in the body. In the problem given in Figure 3-3b, the stress distribution prior to the introduction of the crack (the "uncracked" stress) is assumed to be known, and the surface tractions on the plane where the crack is to appear are denoted as  $T_i^*$ . The tractions  $T_i^*$  are stresses which when applied to the crack face of the original problem are just sufficient to close the crack completely. Because the crack is perfectly closed,  $K^{(b)}$  equals zero. Hence, the model problem given in Figure 3-3c is identical to that of the original problem (Figure 3-3a). In this case (Figure 3-3c), the body is treated with zero boundary stresses on  $S_1$ , fixed zero displacements on  $S_2$ , no body forces over  $V$ , and only  $T_i^*$  acting on the crack face. The strain energy ( $U$ ) is simply the work done by  $T_i^*$  on the crack face:

$$U = -\frac{1}{2} \int_L T_i^* u_i ds \quad (3-7)$$

where  $L$  is the crack boundary. The rate of change of  $U$  with crack length for a body of unit thickness is related to stress intensity factor by:

$$\frac{\partial U}{\partial a} = \frac{K^2}{H} \quad (3-8)$$

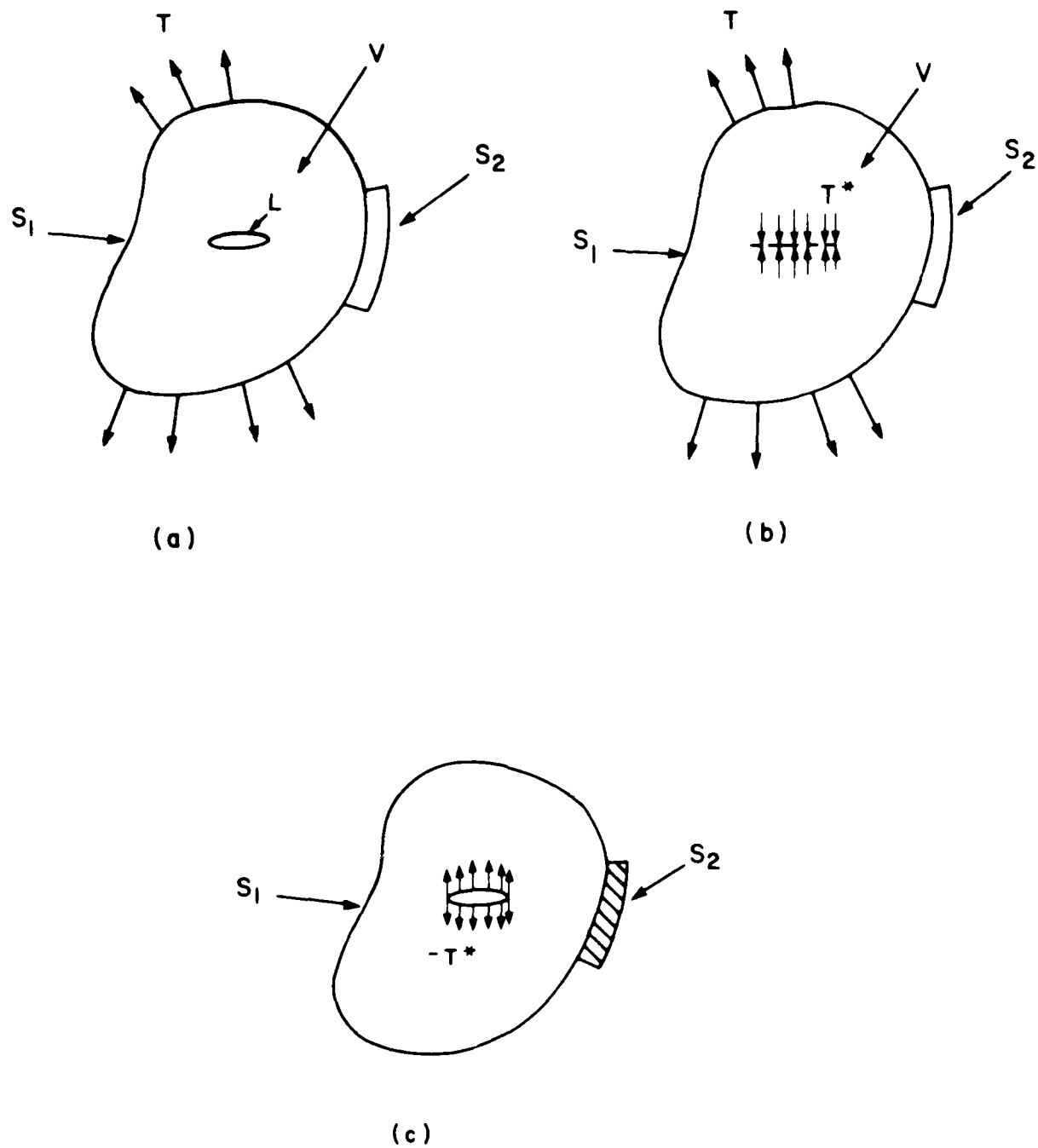


Figure 3-3 - Cracked Body Subject to Three Different Loadings.

The parameter,  $H$ , represents the elastic constants:  $E$  for plane stress and  $E/(1 - \nu^2)$  for plane strain where  $E$  is modulus of elasticity and  $\nu$  is Poisson's ratio.

As will be shown later in the results for thermal heating, it is highly desirable to view the original crack problem of Figure 3-3a as the problem shown in Figure 3-3c. It is preferable to analyze the uncracked body to obtain the solution for  $T^*$  prior to solving for  $K$ . This uncracked analysis permits identification of flaw locations by first observing high stress points in the body as well as determining potential crack propagation paths. Furthermore, in some cases, consideration of other stresses not usually determined by numerical stress analysis is required (e.g., residual stress). These stresses, however determined, can be simply superimposed and substituted in Eq. (3-5).

#### Influence Function Generation

To create an Influence function,  $h(x)$ , it is necessary to obtain the solution for  $T^*$ ,  $u$ , and  $K$  for a simple loading condition by traditional means as suggested by Eqs. (3-7) and (3-8) and to differentiate the crack face displacements with respect to crack length. Development of the theoretical basis is rather complex and involves a deep understanding of analytic function theories (3) or a sophisticated understanding of energy principles of elasticity (4). A clear depiction of the theory is possible by considering two cases of loading on the same body with the following results:

- $K^{(1)}$  Is the stress intensity factor for Case 1
- $u^{(1)}$  Is the displacement vector throughout the body for Case 1
- $T^{(2)}$  Is the stress vector applied by the boundary of the body for Case 2
- $F^{(2)}$  Is the body force acting within the body for Case 2

The results of the theoretical analysis (4) show that for Case 2 the stress intensity factor is given by:

$$K^{(2)} = \frac{H}{2K^{(1)}} \left\{ \int_S T^{(2)} \frac{\partial u^{(1)}}{\partial a} ds + \int_A F^{(2)} \frac{\partial u^{(1)}}{\partial a} da \right\} \quad (3-9)$$

where  $S$  represents the boundary of the body and  $A$  is the area of the body. Since the solution of any crack problem can be reduced to the solution of the same geometry with the loading on the crack boundary only, we can confine Eq. (3-9) to the case where  $F^{(2)} = 0$ ,  $T^{(2)}$  equal to  $\sigma^{(2)}(x)$ , and the only displacement of relevance in Case 1 is the displacement normal to the crack face  $u_n^{(1)}$  over the region of the crack boundary. The expression for  $K^{(2)}$  then becomes:

$$K^{(2)} = \frac{H}{K^{(1)}} \int_0^a \sigma^{(2)} \frac{\partial u_n}{\partial a} dx \quad (3-10)$$

Comparison of Eq. (3-10) with Eq. (3-5) gives the general form of the influence function as:

$$h(x) = \frac{H}{K^{(1)}} \frac{\partial u_n}{\partial a} \quad (3-11)$$

Once  $h(x)$ , the influence function, and  $\sigma(x)$ , the "uncracked" stress acting along the hypothetical crack plane, are known, the stress intensity factor can be calculated by simple numerical integration. This integration can easily be accomplished on a desktop computer.

## INFLUENCE FUNCTIONS FOR TWO CRACKED BODY GEOMETRIES

### Through Cracked Infinite Plate

The influence function for a through crack in an infinite plate shown in Figure 3-4 was derived from the uniform tension solutions given by Irwin (9) or Erdogan (10) where stress functions were used to establish the following:

$$K = \sigma\sqrt{\pi a} \quad (3-12)$$

$$u(x) = \frac{2}{H} x^{-1/2} (2a - x)^{1/2} \sigma$$

From Eq. (3-11), the influence function for a crack over the region  $0 \leq x \leq 2a$  under Mode I loading is:

$$h_I(x) = (\pi a)^{-1/2} \left( \frac{x}{2a - x} \right)^{1/2} \quad (3-13a)$$

for a crack tip located at  $x = 2a$ , and

$$h_I(x) = (\pi a)^{-1/2} \left( \frac{2a - x}{x} \right)^{1/2} \quad (3-13b)$$

for a crack tip at  $x = 0$ . The influence function for Mode II and Mode III loadings are of the same form as Eq. (3-13), hence:

$$h_I = h_{II} = h_{III} \quad (3-14)$$

The solution for  $K_I$  or  $K_{III}$  follows from Eq. (3-5) but with the stress distributions for in-plane ( $\sigma_{xz}$ ) or out-of-plane ( $\sigma_{xy}$ ) shear stress distribution substituted for the normal stress  $\sigma_z(x)$ .

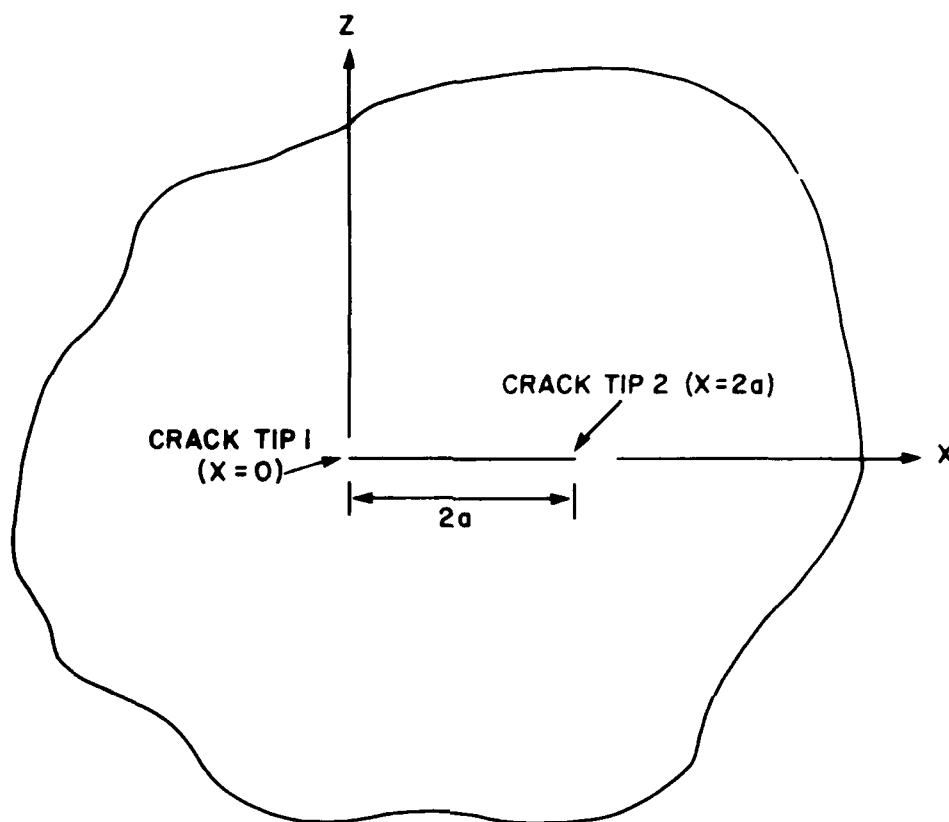


Figure 3-4 - Through Cracked Infinite Panel of Uniform Thickness.

### Edge Cracked Plate

The influence function for an edge cracked plate of finite thickness was derived by Bueckner (11) for the geometry shown in Figure 3-5. A series approximation was used to obtain the function with a reported accuracy of 1 percent for  $0 \leq a/w \leq 0.5$  (i.e., crack penetrations up to one-half the plate thickness). The resulting influence function for Mode I loading is:

$$h_I(x) = (2/\pi)^{1/2} (a-x)^{1/2} \left[ 1 + M_1 \left(1 - \frac{x}{a}\right) + M_2 \left(1 - \frac{x}{a}\right)^2 \right] \quad (3-15)$$

where,

$$M_1 = A_1 + B_1 (a/w)^2 + C_1 (a/w)^6$$

$$M_2 = A_2 + B_2 (a/w)^2 + C_2 (a/w)^6$$

$$A_1 = 0.6147, B_1 = 17.1844, C_1 = 8.7822$$

$$A_2 = 0.2502, B_2 = 3.2889, C_2 = 70.0444$$

For the case of edge crack in a half space, the coefficients become

$M_1 = A_1$  and  $M_2 = A_2$  which simplifies the expression for  $h_I(x)$ .

Equation (3-15) in conjunction with the general stress distribution,  $\sigma_z(x)$ , can be integrated according to Eq. (3-5) for  $0 \leq x \leq a$  to obtain the stress intensity factor.

### Verification of Solutions

The solution of stress intensity factor for the two influence functions was accomplished by numerical integration of Eq. (3-5). A simple rectangular rule was used to perform the integration. Because  $h(x)$  is singular at  $x = a$ , a nonuniform integration grid was used that refines the integration steps as  $x$

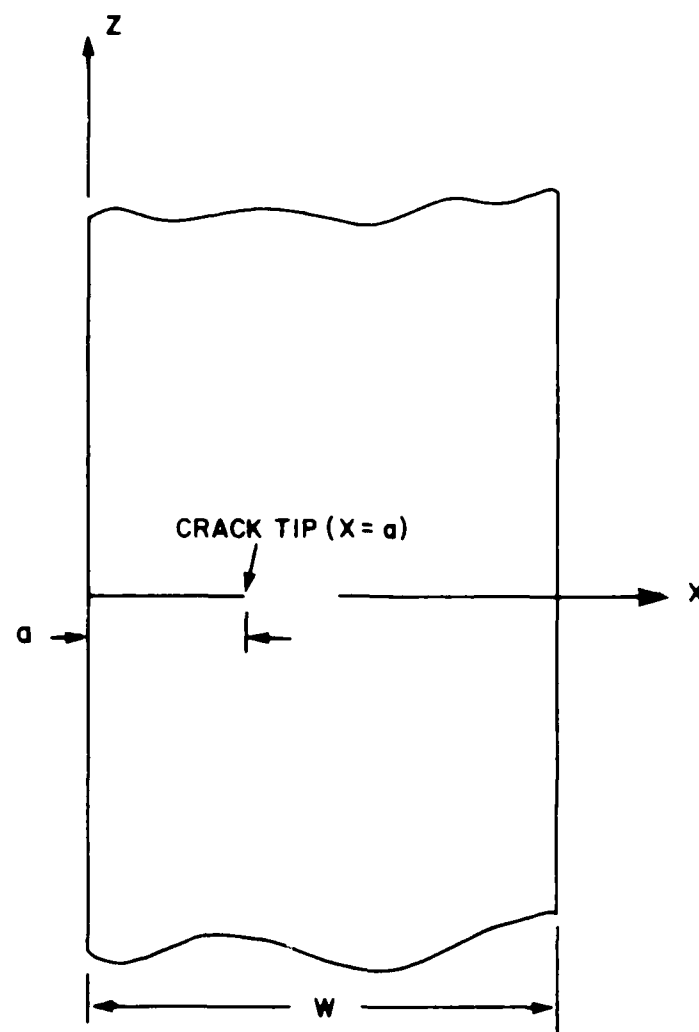


Figure 3-5 - Geometry For Edge Cracked Plate.

approaches the crack tip. Up to 30 integration points were used in the numerical procedure.

The accuracy for the program was verified by comparing the numerical results for the case of uniform tension to that of known values given in the literature (12). This comparison is shown in Figure 3-6 for both flaw models. Very good agreement between the numerical algorithm and the literature results is observed.

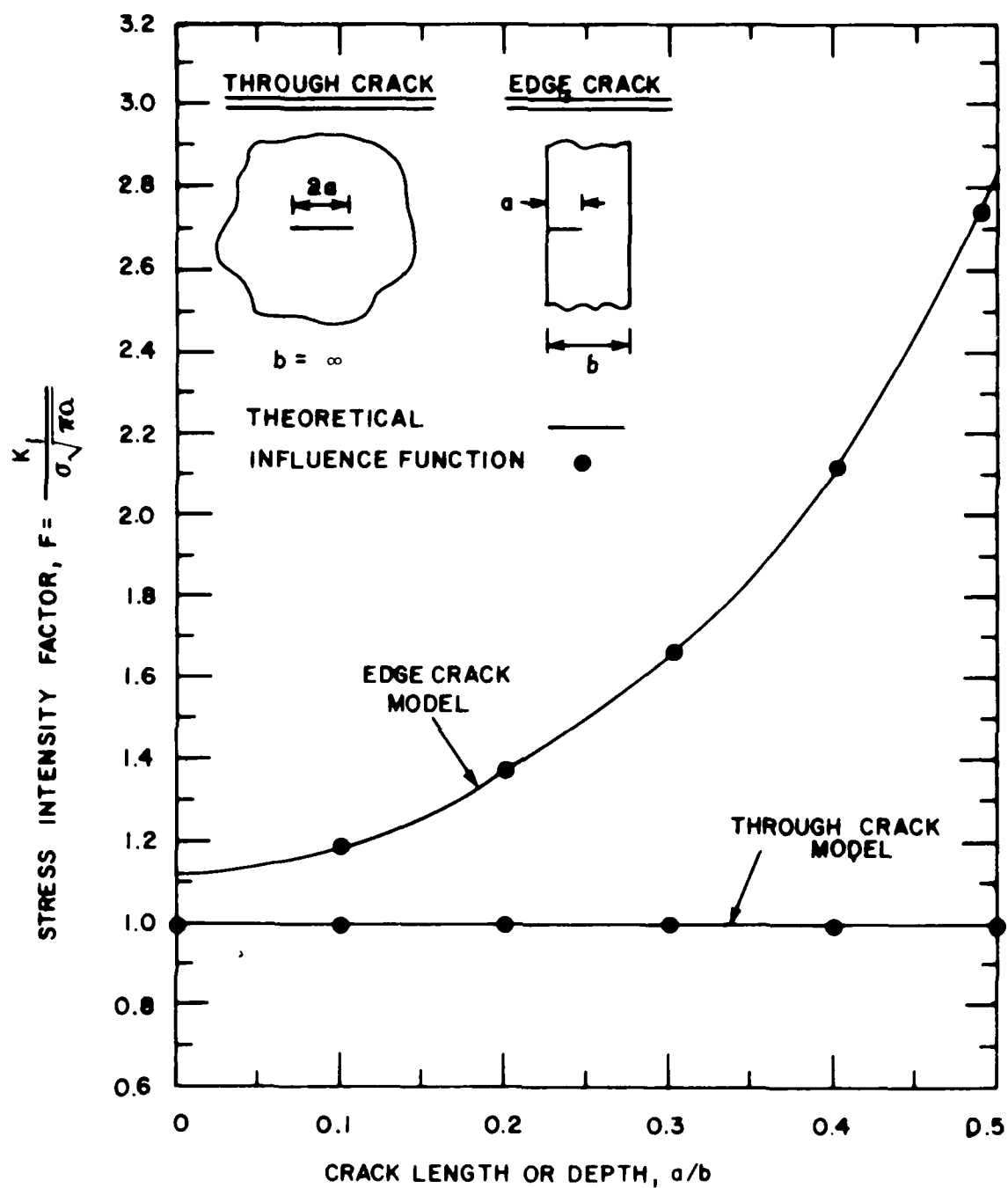


Figure 3-6 - Comparison of Numerical Results From Influence Function Method With Theory For the Case of Uniform Tension.

## Section 4

### THERMAL ANALYSIS MODELS

#### INTRODUCTION

As described in Section 3, the stress intensity factor model requires the thermal stress distribution for the solid. In classical thermal stress analysis, the heat transfer solution is decoupled from the mechanics solution since thermal deformations usually are small and can be neglected in the heat transfer analysis. Although in severe thermal conditions the deformations could be large, the determination of stress herein will be restricted to small displacements and no phase change so that the decoupling of the two problems is acceptable.

The classical representation of heat flow in a three-dimensional solid is given by:

$$\rho C \frac{\partial T}{\partial t} = \frac{\partial}{\partial x} \left( k \frac{\partial T}{\partial x} \right) + \frac{\partial}{\partial y} \left( k \frac{\partial T}{\partial y} \right) + \frac{\partial}{\partial z} \left( k \frac{\partial T}{\partial z} \right) + G \quad (4-1)$$

where  $\rho$  is the material density,  $C$  is the specific heat,  $T$  is the temperature,  $t$  is time, and  $k$  is thermal conductivity. The function  $G$  is the energy produced per unit volume per unit time. In Eq. (4-1),  $\rho$ ,  $C$ , and  $k$  are considered functions of both position and temperature and  $G$  is a function of position and time. This equation is a statement that the rate at which energy accumulates in a volume is equal to the net flow of heat across the surfaces of that volume plus the rate at which heat is produced within the volume.

The solution of Eq. (4-1) in conjunction with the appropriate boundary conditions and initial conditions gives the transient temperature response throughout the solid. We, therefore, seek solutions of Eq. (4-1) for the cases of laser irradiation and aerodynamic heating so that the desired thermal stresses can be computed.

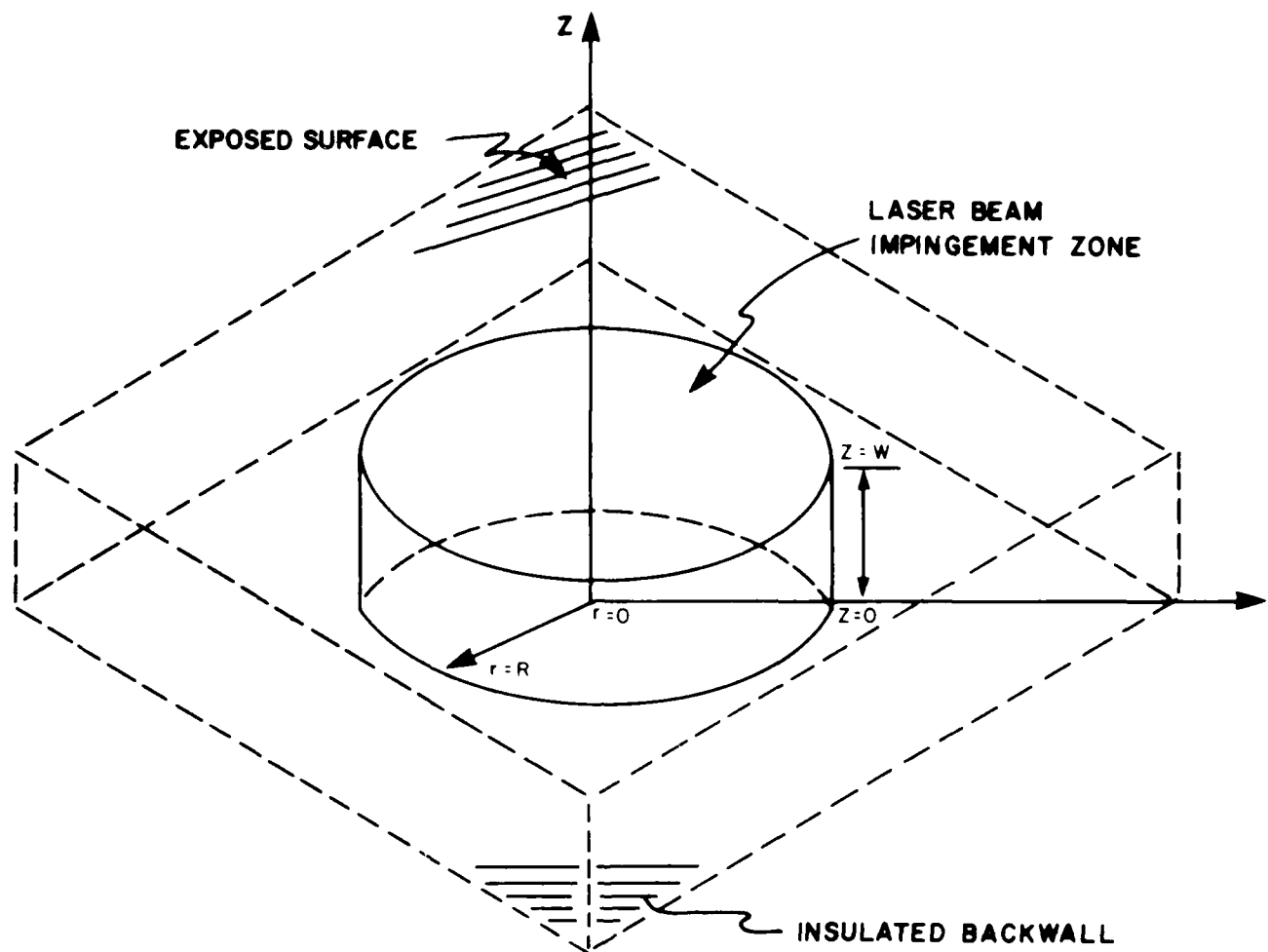
One of the most important effects of intense heating by laser irradiation is the conversion of the electromagnetic wave energy in the beam into thermal energy in the material (13). The rate and source of production of heat by the laser will yield the function  $G$ . For metals exposed to a continuous beam at a wave length of approximately  $10\text{ }\mu\text{m}$ , energy absorption occurs in a very thin layer at the surface. It then becomes convenient to obtain solutions for Eq. (4-1) with  $G = 0$  but with a specified heat flux at the surface boundary. Hence, for continuous wave radiation by a  $\text{CO}_2$  laser (wave length of  $10.6\text{ }\mu\text{m}$ ), the laser beam impingement problem can be treated similar to aerodynamic heating in that the impinging heat flux constitutes a boundary condition. As will be discussed later, other surface effects, such as reradiation of energy and heat loss due to convection from the surface, must also be included as boundary conditions.

## RADIAL HEAT TRANSFER IN A SEMI-INFINITE PLANE

### Governing Equations

The representation of the laser beam impingement plane is modelled as a two-dimensional radial plane. Figure 4-1 illustrates a portion of a semi-infinite metal plate of thickness,  $w$ , with its exposed surface irradiated by a laser beam of radius,  $R$ . A cylindrical coordinate system  $(r, \theta, z)$  is also shown with the  $z$ -axis coincident with the axis of the laser beam and the origin located at the metal plate back wall.

In addition to the impinging laser beam, the exposed surface ( $z = w$ ) also experiences two other modes of heating--convective cooling (or heating) by moving air at all values of  $r$  and surface reradiation at all values of  $r$ . It is assumed that the back wall ( $z = 0$ ) is insulated at all values of  $r$ . If the laser beam is axisymmetric about  $z$  and the convection coefficient is constant, then the resulting heat conduction within the metal is also axisymmetric with the result that the metal temperature at any instant in time will be a function of  $r$  and  $z$  but not angular position about the  $z$  axis.



Metal plate thickness  $w$

Radius of impinging laser beam =  $R$

Boundary conditions:

$z = 0, 0 \leq r \leq \infty \rightarrow$  Insulated

$z = w, 0 \leq r \leq R \rightarrow$  Laser beam impingement

$0 \leq r \leq \infty \rightarrow$  Convective cooling and surface reradiation

Figure 4-1 - Schematic of Laser Beam Impingement Area on Exposed Metal Surface.

The time varying heat transfer in the metal plate is described as follows. Initially, at time  $t < 0$ , the plate is at a uniform temperature throughout because the convective cooling (or heating) and exposed surface reradiation are uniform over the entire surface. Since the back wall is adiabatic, there is no localized source of energy anywhere with the result that no temperature gradients are promoted. At the time  $t = 0$ , the laser beam strikes the exposed surface over the circular area of radius,  $R$ . The beam may be constant or variable with time. The high level of energy associated with the beam is conducted down into the metal and outward in the radial direction. Metal temperatures at  $z = w$  and  $r \leq R$  rise rapidly initially. Temperatures in depth and for  $r > R$  then start to increase as the radial conduction commences. Counteracting the laser beam energy source are the two energy sinks provided by surface reradiation and convective cooling.

Due to the heat transfer events described above, the temperature field in the metal plate is two-dimensional and time dependent,  $T = T(r, z, t)$ . It can be shown from Eq. (4-1) that this temperature field in cylindrical coordinates with no internal heat generation is governed by the following partial differential equation:

$$\rho C \frac{\partial T}{\partial t} = \frac{1}{r} \frac{\partial}{\partial r} \left( r k \frac{\partial T}{\partial r} \right) + \frac{\partial}{\partial z} \left( k \frac{\partial T}{\partial z} \right) \quad (4-2)$$

where,

$\rho = \rho(T) =$  Metal density

$C = C(T) =$  Metal specific heat

$k = k(T) =$  Metal thermal conductivity

Note that Eq. (4-2) is formulated with the metal thermophysical properties  $\rho$ ,  $C$ , and  $k$  allowed to vary with temperature. Of course, Eq. (4-2) is subject to both an initial condition:

$$T = T(r, z, 0) \quad (4-3)$$

for all  $z$  and  $r$  values, and the heat flux boundary conditions at  $z = 0$  and  $z = w$  already described:

$$\frac{T(r, 0, t)}{\partial z} = 0 \quad (4-4)$$

$$-k \frac{\partial T(r, w, t)}{\partial z} = Q \quad (4-5)$$

where  $Q$  is the net heat flux from the surface energy balance. The surface energy balance in Eq. (4-5) is of the general form:

$$Q = \dot{q}''(r, w, t) = -\alpha_s \dot{q}''_{\text{laser}} + \dot{q}''_{\text{convection}} + \dot{q}''_{\text{radiation}} \quad (4-6)$$

where  $\alpha_s$  is the surface absorptance. Thus, for the laser impingement region ( $0 \leq r \leq R$ ):

$$-k \frac{\partial T}{\partial z} = -\alpha_s \dot{q}''_{\text{laser}} + h(T - T_\infty) + \sigma_s \epsilon_m (T^4 - T_0^4) \quad (4-7)$$

while outside of the laser impingement region ( $R < r \leq \infty$ ):

$$-k \frac{\partial T}{\partial z} = h(T - T_\infty) + \sigma_s \epsilon_m (T^4 - T_0^4) \quad (4-8)$$

where, in the equations above,  $h$  is the surface transfer coefficient,  $T_\infty$  is the air temperature,  $T_0$  is the remote temperature for radiation,  $\sigma_s$  is the Stefan-Boltzmann Constant, and  $\epsilon_m$  is surface emittance.

Since Eq. (4-2) is nonlinear due to the variation of thermophysical properties with temperature, the most practical means of solution is to use a finite

difference method which is based on a network of discrete nodes in the region of the metal plate where significant heat conduction occurs.

### Numerical Solution

In this work, the approach described by Griffiths, et al., (1) has been followed. Figure 4-2 illustrates a lumped mass nodal network around a surface node. This node experiences heat conduction to or from all adjacent Nodes 1, 2, and 3 and heat fluxes to or from its exposed surface due to the three mechanisms identified. As derived by Griffiths, et al., (1), the incremental temperature rise at the surface,  $\Delta T_i$ , for an increment in time,  $\Delta t$ , is given by:

$$\Delta T_i = \left[ \sum_j^3 K_{ij} (T_j - T_i) + r_i \Delta r_i \alpha_s \dot{q}''_{\text{laser}} + r_i \Delta r_i \sigma_s \epsilon_m (T_0^4 - T_i^4) + r_i \Delta r_i h (T_\infty - T_i) \right] \frac{\Delta t}{r_i \Delta r_i \Delta z_i \rho_i C_i} \quad (4-9)$$

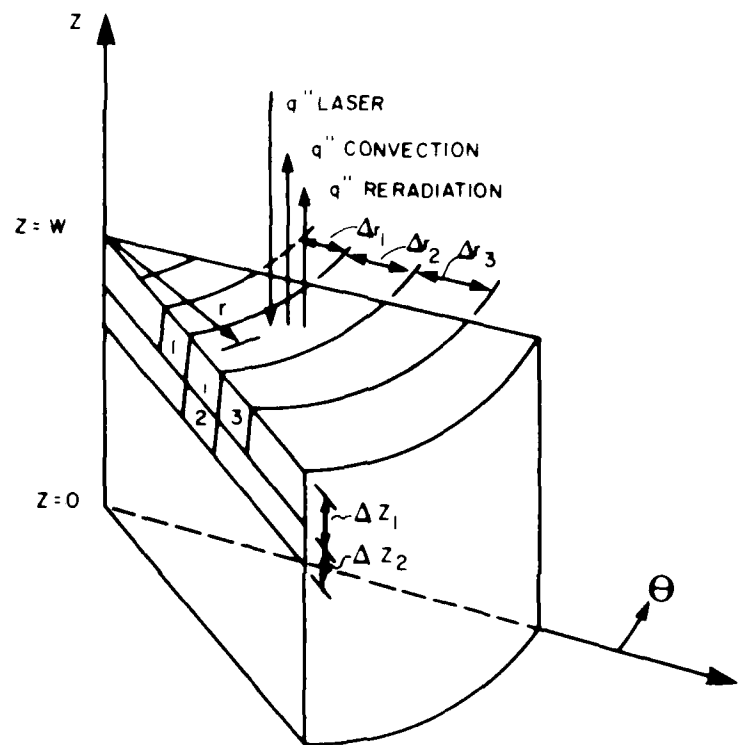
where, for the radial direction:

$$K_{ij} = 2A_{ij} \left[ \frac{\Delta r_i}{k_i} + \frac{\Delta r_j}{k_j} \right]^{-1} \quad (4-10)$$

$$A_{ij} = \frac{r_i + r_j}{2} \Delta z_i \quad (4-11)$$

and, for the vertical direction:

$$K_{ij} = 2A_{ij} \left[ \frac{\Delta z_i}{k_i} + \frac{\Delta z_j}{k_j} \right]^{-1} \quad (4-12)$$



NOTE:  $\dot{q}''$  = Heat Flux = Energy per unit area per unit time.

Figure 4-2 - Lumped Mass Heat Conduction Model.

$$A_{ij} = r_i \Delta r_i \quad (4-13)$$

For a subsurface node, Eq. (4-8) simplifies to:

$$\Delta T_i = \left[ \sum_j^4 K_{ij} (T_j - T_i) \right] \frac{\Delta t}{r_i \Delta r_i \Delta z_i \rho_i C_i} \quad (4-14)$$

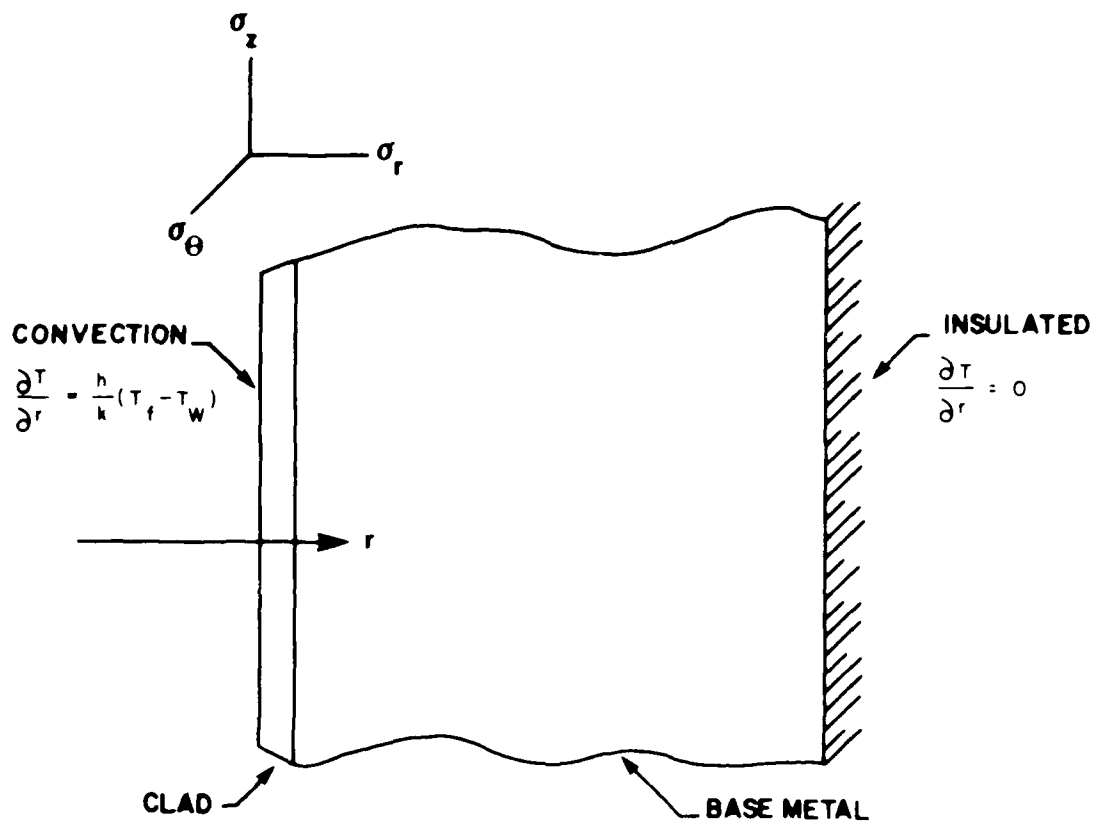
where  $K_{ij}$  is defined by Eq. (4-10) for the radial direction and by Eq. (4-12) for the vertical direction. Equations (4-9) and (4-14) are the desired finite difference approximations to Eq. (4-2).

As discussed by Griffiths, et al. (1), the right hand side of Eq. (4-9) is evaluated at present time and the left hand side is treated as an incremental change between present temperature and future temperature after elapsed time,  $\Delta t$ . Mathematically, this is an explicit (rather than implicit) numerical solution approach. Because of the thinness of aircraft skin relative to other dimensions, the through thickness heat flow is neglected in the present investigation. This assumption will allow for a simplification of the method to a one-dimensional model.

#### THROUGH THICKNESS HEAT FLOW IN A CURVED SHELL

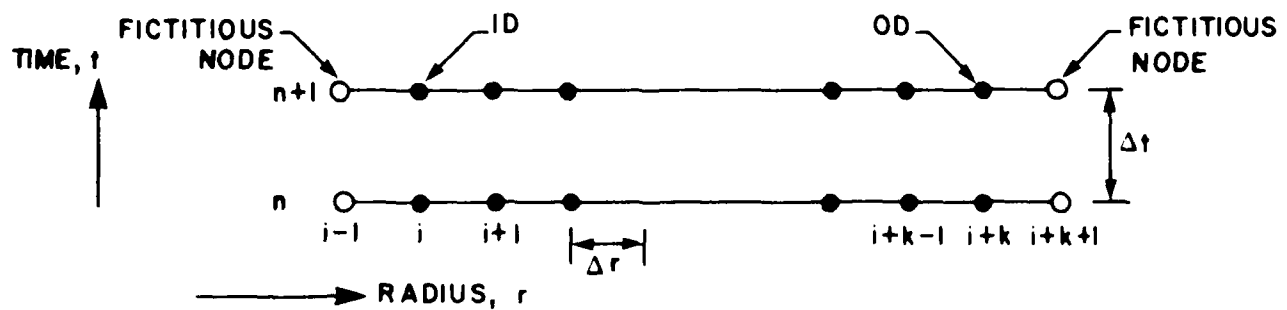
##### Governing Equations

The thermal response resulting from one-dimensional heat flow through the thickness of a curved cylindrical shell was used to model uniform aerodynamic heating of the leading surface. The model geometry is shown in Figure 4-3.



$T$  = Temperature  
 $r$  = Radius  
 $h$  = Heat transfer coefficient  
 $k$  = Thermal conductivity of the surface  
 $T_\infty$  = Fluid temperature

(a) Thermal Model Geometry and Boundary Conditions.



(b) Finite Difference Model.

Figure 4-3 - Thermal Model Geometry.

The solution for the transient response of two concentric shells of dissimilar materials involves solving a parabolic partial differential equation of the form:

$$\frac{\partial^2 T}{\partial r^2} + \frac{1}{r} \frac{\partial T}{\partial r} = \frac{1}{\alpha_t} \frac{\partial T}{\partial t} \quad (4-15)$$

where,

$t$  = Time

$r$  = Radial coordinate

$T$  = Temperature,  $T(r, t)$

$\alpha_t$  = Thermal diffusivity

The modelling of two-layer construction will allow the analysis of aircraft structures where a thermal protective skin is applied to the outer surface.

The boundary conditions are nonhomogeneous and require that shell inside ( $r = r_i$ ) and outside ( $r = r_o$ ) surfaces transfer heat between the metal surface and the environment:

$$\frac{\partial T}{\partial r} = \frac{h_i}{k_i} (T_\infty - T_{wi}), \text{ at } r = r_i \quad (4-16)$$

$$\frac{\partial T}{\partial r} = \frac{h_o}{k_o} (T_\infty - T_{wo}), \text{ at } r = r_o \quad (4-17)$$

where,

$h_i, h_o$  = Surface heat transfer coefficients (inside and outside)

$k_i, k_o$  = Thermal conductivity of surface materials

$T_{wi}, T_{wo}$  = Metal surface temperatures

$T_\infty$  = Air or gas temperature

The initial condition for the analysis is:

$$T(r, 0) = T_0 = \text{Constant} \quad (4-18)$$

#### Numerical Solution

The solutions of Eqs. (4-15) through (4-18) are accomplished using a finite difference method based on the Crank-Nicolson technique. This is an implicit approach, and the temperatures are obtained by solving a set of simultaneous linear equations (14). The nodal point scheme for the difference equations is shown in Figure 4-3. By defining the temperature  $\hat{T}(r, t) = T(R, t) - T(r, 0)$ , the difference equations  $\hat{T}_{i,n}$  will represent the temperature at the  $i^{\text{th}}$  point into the model and at the  $n^{\text{th}}$  step where radial distance,  $r = i\Delta r$  and time  $t = n\Delta t$ . For simplicity, the " $\hat{\phantom{x}}$ " notation will be dropped in the difference equations which will follow.

Two additional or fictitious node points are used so that a central difference relation can be formulated at the inside and outside shell walls. This yields three difference equations (one for each node at the wall and one for an

Internal node). The finite difference equation for the convective boundary condition is:

$$\frac{T_{i+1,n} - T_{i-1,n}}{2\Delta r} = \frac{h}{k} (T_{\infty} - T_{i,n}) \quad (4-19)$$

The finite difference equation for the partial differential equation at the wall including the convective boundary conditions is:

$$T_{i+1,n+1} - \left(1 + \frac{\Delta r^2}{\alpha_t \Delta t}\right) T_{i,n+1} - \Delta r \gamma(t)_{n+1} + \frac{\Delta r \gamma(t)_{n+1}}{2i} + \quad (4-20)$$

$$T_{i+1,n} - \left(1 - \frac{\Delta r^2}{\alpha_t \Delta t}\right) T_{i,n} - \Delta r \gamma(t)_n + \frac{\Delta r \gamma(t)_n}{2i} = 0$$

where  $\gamma(t)$  is:

$$\frac{h}{k} (T_{\infty} - T_{i,n}) \quad (4-21)$$

The finite difference equation for an internal node, say the  $i+3$  node as an example, is:

$$\left(1 - \frac{1}{2i}\right) T_{i+2,n+1} - 2\left(1 + \frac{\Delta r^2}{\alpha_t \Delta t}\right) T_{i+3,n+1} + \left(1 + \frac{1}{2i}\right) T_{i+4,n+1} \quad (4-22)$$

$$+ \left(1 - \frac{1}{2i}\right) T_{i+2,n} - 2\left(1 - \frac{\Delta r^2}{\alpha_t \Delta t}\right) T_{i+3,n} + \left(1 + \frac{1}{2i}\right) T_{i+4,n} = 0$$

For the case when an insulated boundary ( $h = 0$ ) is assumed, the finite difference equation for the insulated boundary condition is (central difference):

$$\frac{T_{i+k+1,n} - T_{i+k-1,n}}{2\Delta r} = 0$$

This results in a difference equation for the node at the wall which includes the insulated boundary condition as:

$$T_{i+k-1,n+1} - \left(1 + \frac{\Delta r^2}{\alpha_t \Delta t}\right) T_{i+k,n+1} + T_{i+k-1,n} - \left(1 - \frac{\Delta r^2}{\alpha_t \Delta t}\right) T_{i+k,n} = 0 \quad (4-23)$$

A special situation arises for the case of an internal node at the interface of the dissimilar materials. For this node, the thermal properties of the base material are assumed as an approximation, although a more exact solution would involve conservation of heat transfer across the boundary between the two materials. It should also be noted that the temperatures at the convective wall ( $T_w$ ) may oscillate in time about a central ("correct") value when the heat transfer coefficient is a very large value. This phenomenon does not affect the accuracy of the interior points and may be avoided by using a smaller time increment (14).

#### THERMAL STRESS ANALYSIS

Once the temperature distribution is known, the elastic stress in a two-dimensional solid can be determined by satisfying the equations of equilibrium and compatibility in conjunction with the boundary conditions. In treating the true thermal stress problem (i.e., without body forces), the

equilibrium equations will automatically be satisfied if a stress function,  $\varphi$ , can be found such that:

$$\sigma_x = \frac{\partial^2 \varphi}{\partial y^2}, \quad \sigma_y = \frac{\partial^2 \varphi}{\partial x^2}, \quad \sigma_{xy} = \frac{\partial^2 \varphi}{\partial x \partial y} \quad (4-24)$$

where  $\sigma_x$ ,  $\sigma_y$ , and  $\sigma_{xy}$  are the component stresses.

Considering the plane stress case, the strain ( $\epsilon$ ) can be expressed in terms of the stress function through the use of stress strain relations. Substitution of these strains into the compatibility equation:

$$\frac{\partial^2 \epsilon_x}{\partial y^2} + \frac{\partial^2 \epsilon_y}{\partial x^2} = \frac{\partial^2 \gamma_{xy}}{\partial x \partial y} \quad (4-25)$$

yields the inhomogeneous biharmonic equation:

$$\nabla^4 \varphi + E \alpha_e \nabla^2 T = 0 \quad (4-26)$$

where  $E$  is the modulus of elasticity,  $\alpha_e$  is the coefficient of thermal expansion, and  $\nabla^2$  notation represents the Laplacian operator. Solution of Eq. (4-26) for the stress function with the appropriate boundary conditions will give resultant stresses from the equilibrium equations.

Although most thermal stress problems are treated by approximate solution methods, a class of exact solutions will be exploited herein to simplify the model (15). When the temperature does not vary in one direction, it can be assumed that the stress due to heating does not vary in that direction. For these simple cases, it is possible to integrate the governing stress equations above to yield the thermal stress. For the circular plate geometry for laser

heating shown in Figure 4-2, the integral equations for radial and hoop stresses are (16):

$$\sigma_r = \alpha_e E \left[ \frac{1}{b^2} \int_0^b T r dr - \frac{1}{r^2} \int_0^r T r dr \right] \quad (4-27)$$

$$\sigma_\theta = \alpha_e E \left[ -T + \frac{1}{b^2} \int_0^b T r dr + \frac{1}{r^2} \int_0^r T r dr \right] \quad (4-28)$$

where  $E$  and  $\alpha_e$  are constants, the thickness of the plate is also constant and  $b$  is the outer radius of the radial plane where traction free boundary conditions are applied. By introducing cylindrical body curvature, Eqs. (4-27) and (4-28) have been rewritten in terms of the aerodynamic heating problem shown in Figure 4-3 as given below:

$$\sigma_r = \frac{\alpha_e E}{r^2} \left[ \frac{r_o^2 - r_i^2}{r_o^2 - r_i^2} \int_{r_i}^{r_o} T r dr - \int_{r_i}^r T r dr \right] \quad (4-29)$$

$$\sigma_\theta = \frac{\alpha_e E}{r^2} \left[ \frac{r_o^2 - r_i^2}{r_o^2 - r_i^2} \int_{r_i}^{r_o} T r dr + \int_{r_i}^r T r dr - T r^2 \right] \quad (4-30)$$

where  $r_i$  and  $r_o$  are the inner and outer radii.

For the stress solution of each problem (i.e., laser heating or aerodynamic heating), the above equations are integrated at each time step using the nodal

values for  $T(r, t)$  computed from the thermal solution routines. For the model representing aerodynamic heating, as the interface between the dissimilar materials, another node is added so that two nodes at the interface each have the material properties of its respective side. Since, in general, the temperature distributions across the interface will be continuous, the accuracy in the stress calculation at the interface will not be in significant error even though a considerable stress discontinuity could exist at the same point.

## Section 5

### LASER BEAM IRRADIATION ON A FLAT PLANE

#### PROBLEM PARAMETERS

##### Geometry

The problem of laser beam impinging perpendicular on a flat planar surface in the vicinity of a through thickness crack is represented in Figure 5-1. The crack has a total length of  $2a$  and the center of the crack is a distance,  $r_c$ , from the center of the laser beam. The crack is also oriented by the angle,  $\theta_c$ , relative to a radial line connecting the crack center with the laser beam impingement zone. The beam cross section is assumed circular with a radius,  $R$ . The thickness of the plane is defined as  $w$ . The local coordinate system for the crack is the same as depicted earlier in Figure 3-4.

Because of the many variables that can be investigated, most of the geometry parameters are held fixed. Specifically,  $R$  is equal to 2 inches,  $w$  is equal to 0.25 inch, and the ratio  $r_c/R$  is set at two in the analyses that follow. The effect of crack length and its relative angular position on stress intensity factor are analyzed parametrically.

##### Thermal Parameters and Material Properties

The thermal model described in Section 4 requires as input the surface flux imparted by the laser, the absorptivity, the emissivity, and the basic thermal properties of the panel. In the analysis, the panel material properties are taken from typical values for aluminum alloy Type 7075-T6 (1, 17, 18). A summary of the assumed properties is given in Table 5-1. The thermal and mechanical properties listed are at room temperature. In the analysis, the thermal and mechanical properties are assumed not to change with temperature,

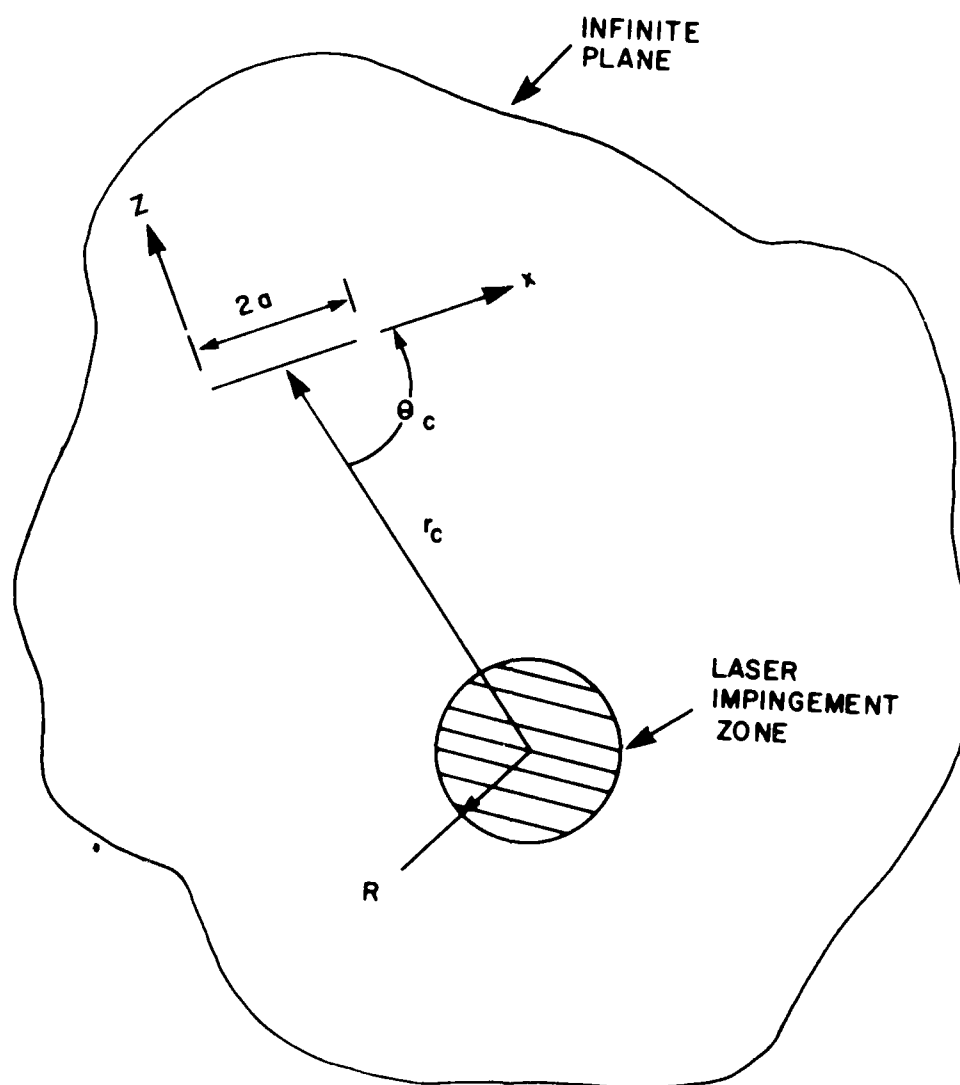


Figure 5-1 - The Geometry of an Infinite Plane Containing a Through Thickness Crack and Subjected to Laser Heating.

Table 5-1  
SUMMARY OF PROPERTIES OF ALUMINUM ALLOY 7075-T6

<u>Property</u>	<u>Assumed Value</u>
Specific Heat, C	0.23 BTU/lb-°F
Density, $\rho$	169 lbs/ft <sup>3</sup>
Thermal Conductivity, k	75 BTU/hr-ft-°F
Thermal Expansion, $\alpha_e$	$13 \times 10^{-6}$ in/in-°F
Poisson's Ratio, $\nu$	0.33
Elastic Modulus, E	$10.3 \times 10^6$ psi
Yield Strength, $\sigma_y$	73 ksi
Ultimate Strength, $\sigma_u$	83 ksi
Liquidus Temperature	1175°F
Solidus Temperature	890°F
Incipient Melting Temperature	990°F

although the temperature solution algorithm can accommodate temperature varying properties.

Two laser radiation fluxes are assumed ( $100 \text{ W/cm}^2$  and  $500 \text{ W/cm}^2$ ) which are capable of being achieved by a large  $\text{CO}_2$  laser. The surface absorption of the aluminum panel can range between 0.6 to 0.9 depending on whether the surface is highly polished or heavily oxidized or painted (19, 20). In this investigation,  $\alpha_s$  is assumed to be 0.8, which represents a painted surface. Further analysis simplification is made by assuming gray body behavior for radiation so that emissivity and absorptivity can be equated. Normally, these parameters are surface condition and wave length dependent and, in general, independent of each other. Remote temperature for radiation losses from the panel is assumed to be absolute zero ( $T_o = -460^\circ\text{F}$ ).

#### STRESS SOLUTIONS

The temperature and stress response of the panel was solved with the finite difference model. The panel was modelled in one dimension with only a single node representing the global z (through thickness) direction. A total of 200 nodes was used in the radial direction to a maximum radius of 20 inches. Hence, the radial spacing between nodes was 0.1 inch. Because of the implicit numerical procedure, several time increments were tried in order to verify numerical stability. It was determined that  $\Delta t = 0.05$  second gave reasonable results. Transient temperature solutions for ten seconds duration were made, however, because of the analysis assumptions, only the solutions up to four seconds are realistic.

The temperature distribution at 0.5 second after the laser flux was applied is shown in Figure 5-2. In this example and the calculations for K that follow, the panel was assumed stationary so heat loss due to convection was zero. For a flux of  $500 \text{ W/cm}^2$ , the metal temperature has risen by more than  $200^\circ\text{F}$  above the initial plate temperature of  $70^\circ\text{F}$ . Because the laser flux is applied uniformly over the region,  $0 \leq r/R \leq 1$ , the temperature profile exhibits a plateau behavior over the irradiated region with a very sharp

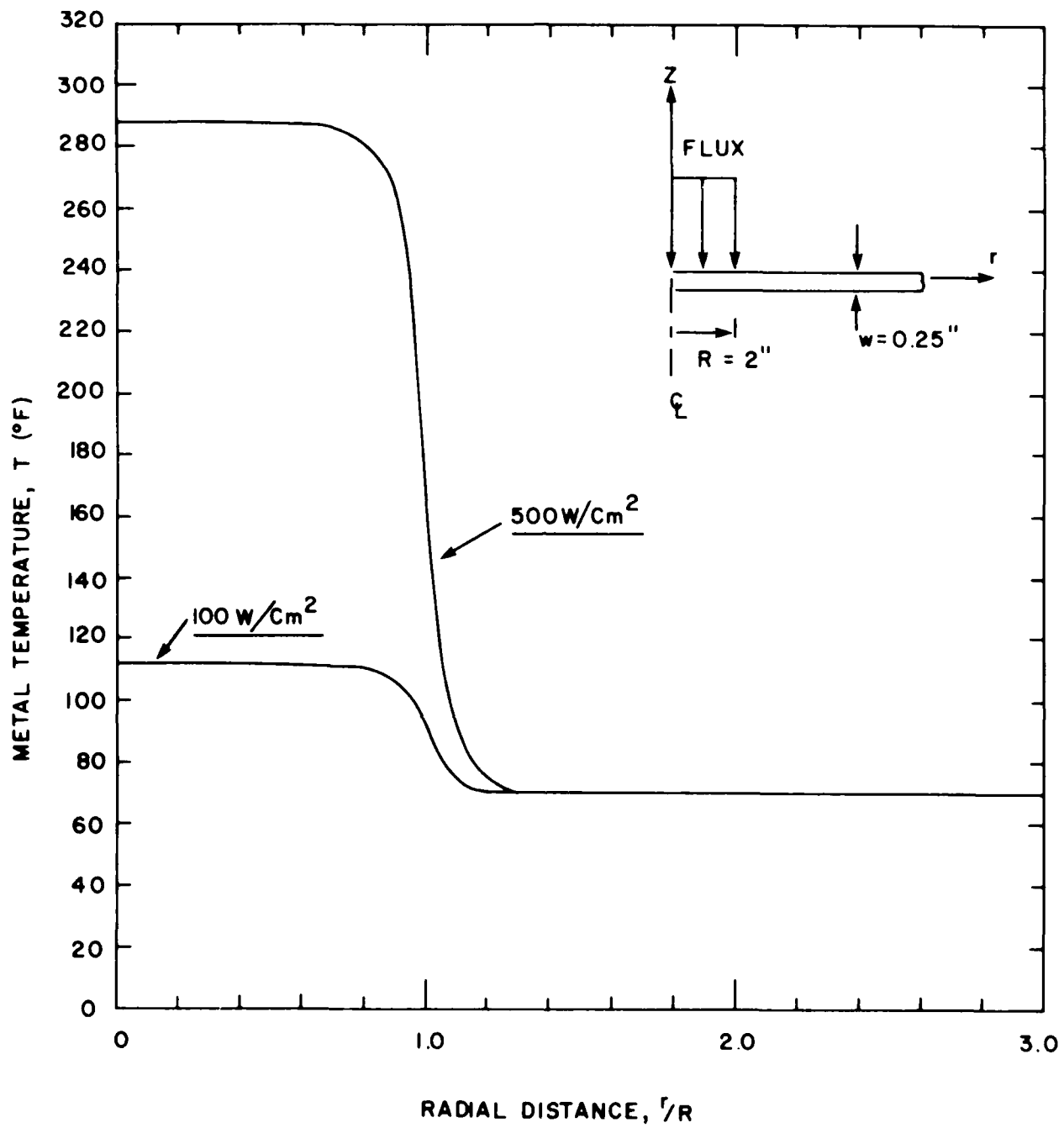


Figure 5-2 - Temperature Distribution For Two Flux Levels at  $t = 0.5$  Second.

attenuation occurring at  $r/R = 1$ . The case of  $100 \text{ W/cm}^2$  flux shows a significantly less severe thermal upset of the plate and comparably lower stresses and stress intensity factor would result.

The radial ( $\sigma_r$ ) and tangential ( $\sigma_\theta$ ) stresses corresponding to the temperature gradients of Figure 5-2 are plotted in Figure 5-3. The radial stresses are everywhere compressive implying that cracks oriented parallel to the laser beam boundary ( $\theta_c = 90^\circ$ ) will not experience positive crack opening forces. Based on the magnitude of the stress components, flaws oriented perpendicular to the beam boundary ( $\theta_c = 0$ ) will have the highest Mode I stress intensity factors. This result is, in part, due to our one-dimensional treatment of the problem, but nonetheless, this observation will be true in most two-dimensional cases.

The highest tensile stresses occur close but just outside the beam boundary and attenuate away as the radial distance away from the beam increases. A time equal to 0.5 second, the peak stress is computed to be 9 ksi for the  $500 \text{ W/cm}^2$  case and about 2 ksi for the  $100 \text{ W/cm}^2$  flux. Because the beam energy is both uniform and continuous in time, the stresses continuously increase in magnitude under the elastic conditions assumed in the model.

#### STRESS INTENSITY FACTORS

The stress intensity factor was calculated by the influence function method described in Section 3. The stress intensity factor for a crack oriented perpendicular to the beam circular boundary is shown in Figure 5-4. Here,  $K$  is plotted as a function of time from the start of laser beam contact. The crack center is located 4 inches from center to the beam and the crack half length is 1 inch (i.e.,  $a = 1$  inch).

The  $K$  level at each crack tip is observed to increase with time as would be expected for a continuously local heating of the plate. The largest  $K$  values are computed for the highest flux case, which is also expected. What is interesting, however, is that the  $K$  level due to heating can be significant,

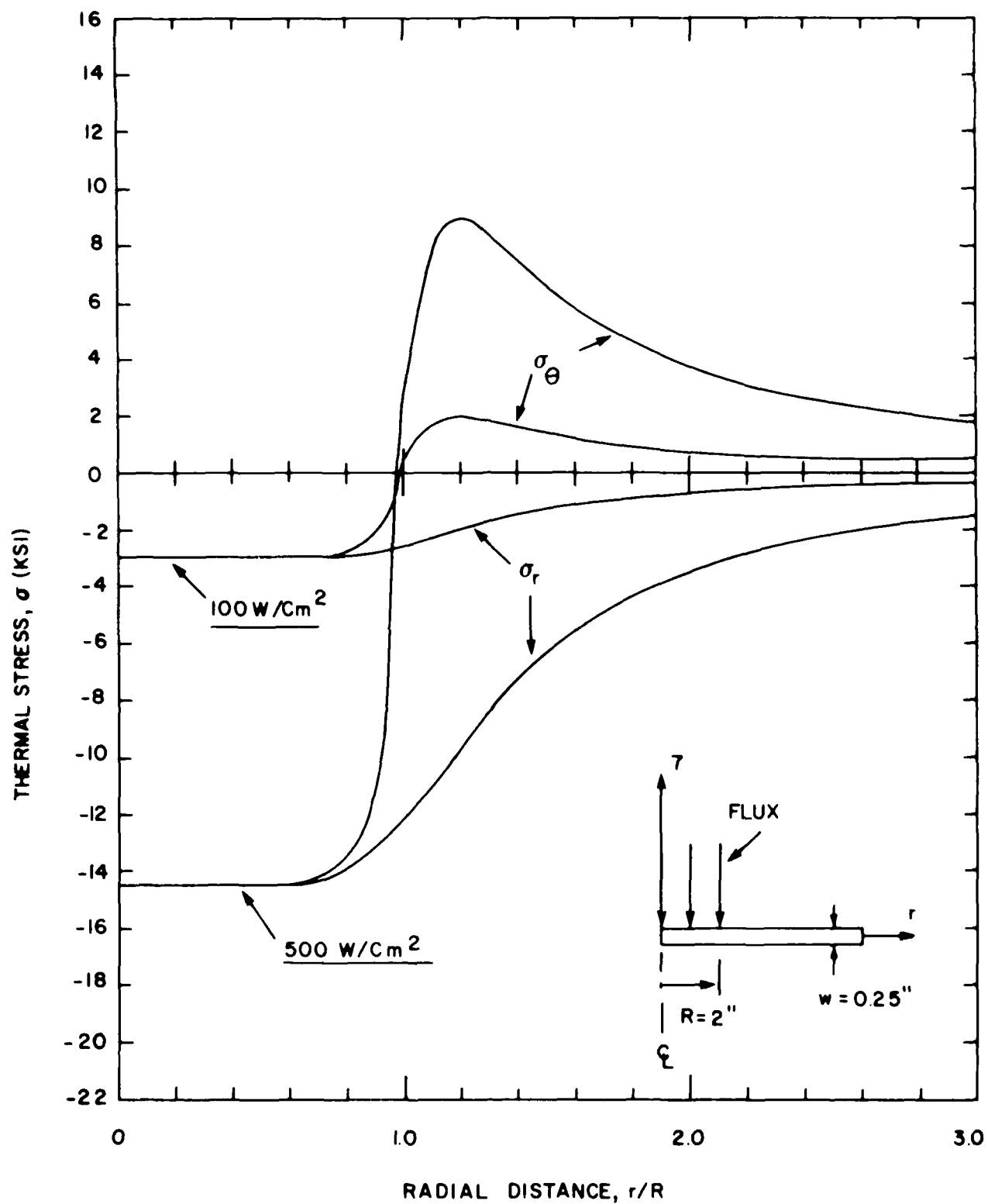


Figure 5-3 - Stress Distribution For Two Laser Flux Levels at  $t = 0.5$  Second.

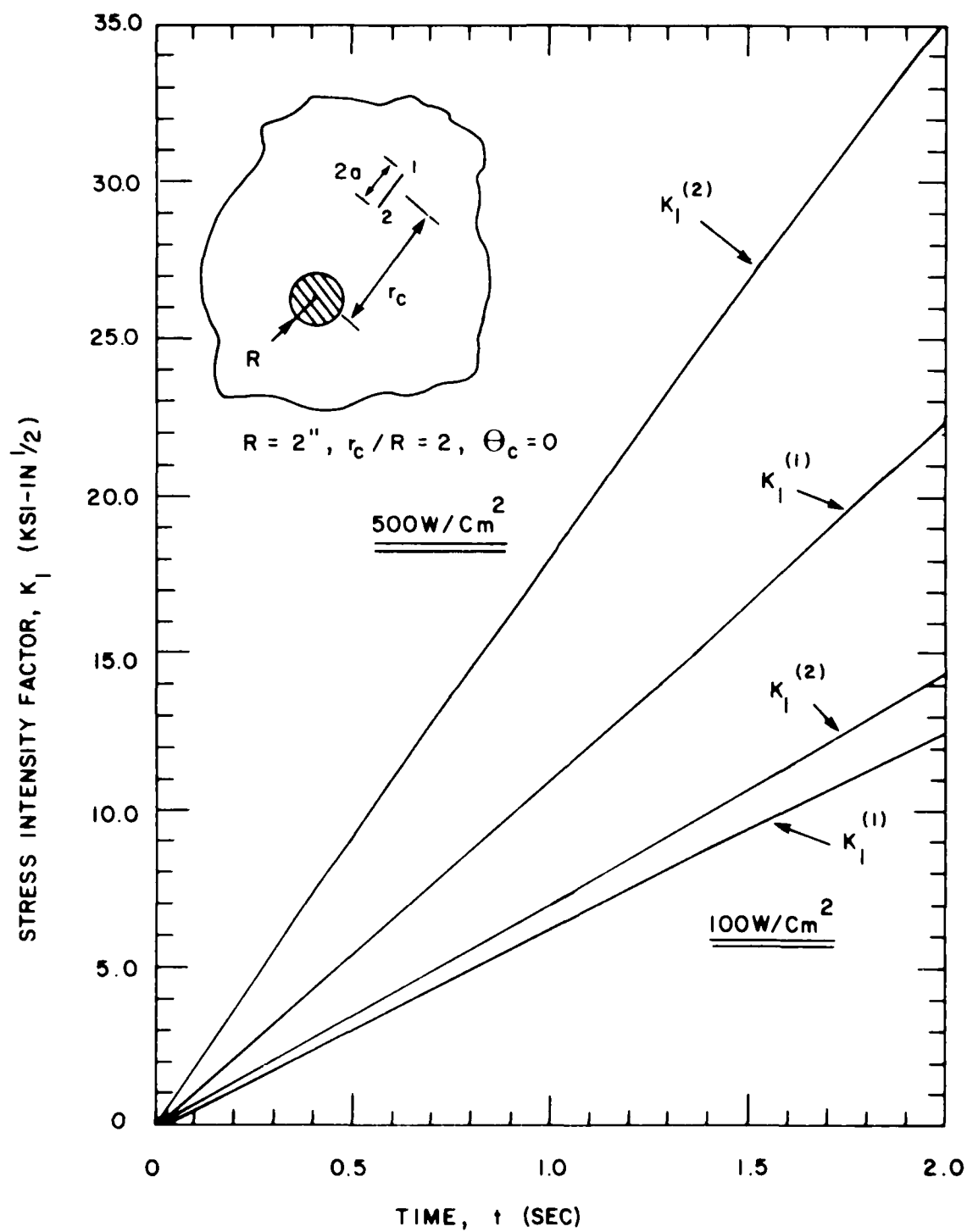


Figure 5-4 - Variation of  $K$  with Time During Laser Irradiation.

up to 20 percent of  $K_{Ic}$  for the material and occurring within the first second of irradiation although a crack of 2 inches in total length would be quite large to remain undetected in a critical airframe member. In any case, it is possible to generate large crack driving forces if the impinging beam is of significant energy and surface area contact.

As shown in Figure 5-4, the  $K$  levels for each crack tip are very nearly equal early for the thermal transient but diverge rapidly as time progresses, especially for the  $500 \text{ W/cm}^2$  flux case. The maximum  $K$  value occurs at the crack tip (Crack Tip 2) closest to the laser heating zone due to the increasing stress gradient in that direction. Unstable fracture initiating at that crack tip would undoubtedly propagate toward the hot spot where it probably would arrest. Although not evaluated in this investigation, the conditions for fracture reinitiation at the remote crack tip can also be determined by selecting appropriate  $r_c/R$  ratios (between zero and two in this example). The influence function method is capable of modeling the flaw for any value of  $r_c$ .

The stress intensity factor as a function of crack length for the stress conditions occurring at 2 seconds for the two laser fluxes is given in Figure 5-5. As the physical crack length is increased, the  $K$  level at each crack tip also increases with the crack tip closest to the beam exhibiting the maximum computed  $K$  value. Although not calculated in this investigation, it would be expected that flaws located closest to the laser irradiated zone but not directly under the heated region would be the most critical based solely on the thermal stress distribution. A proper structural integrity evaluation would combine aerodynamic loads with the thermal loads in order to establish the critical flaw conditions. This feature could be easily added to the present method.

For the case of a crack oriented  $45^\circ$  with respect to  $r_c$ , the crack tip deformation mode is predominately Mode II. The Mode II stress intensity factor is plotted as a function of crack length in Figure 5-6. Comparison of these results with the pure Mode I case of Figure 5-5 shows similar trends and

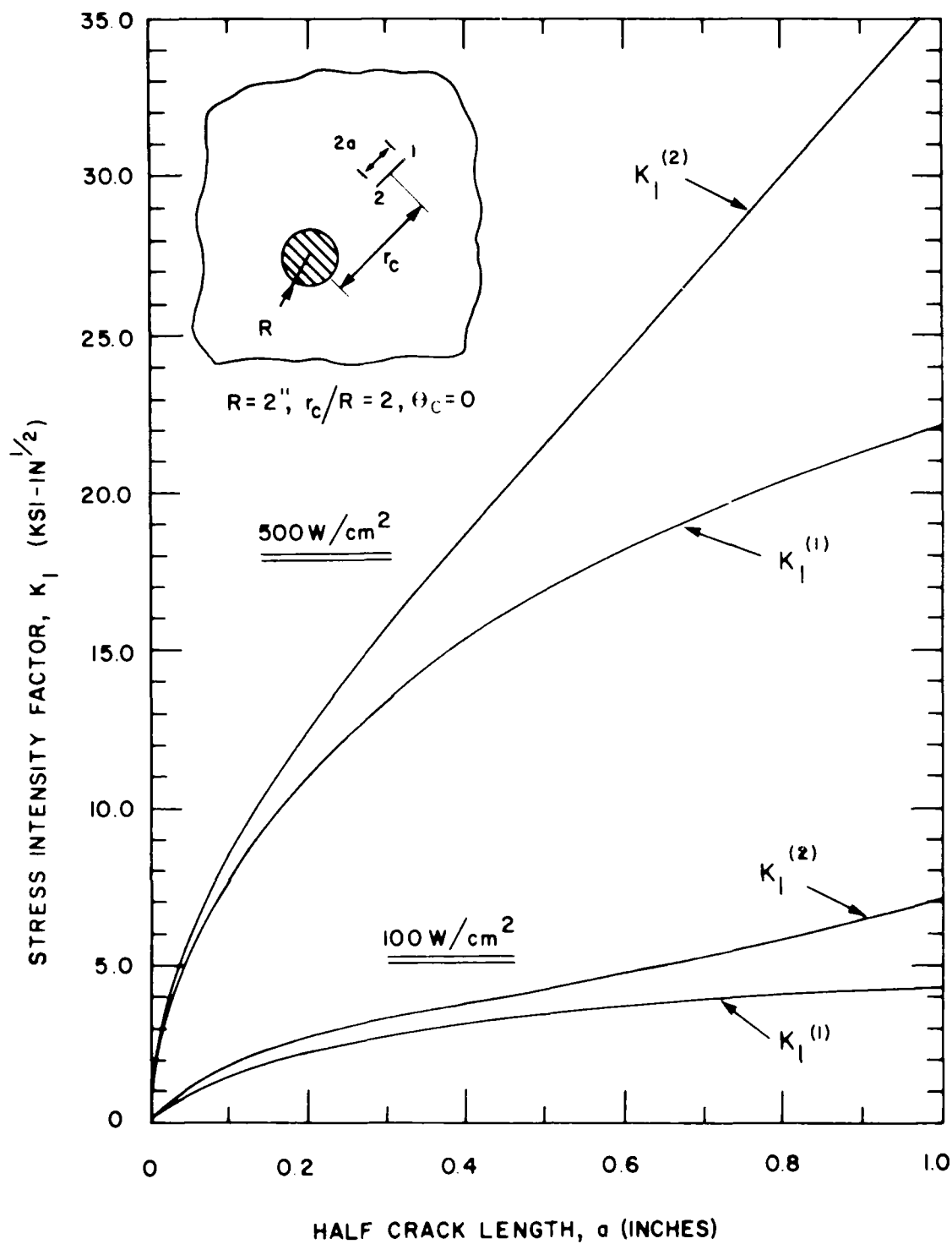


Figure 5-5 - Stress Intensity Factor Versus Crack Length for Two Laser Flux Cases After 2 Seconds of Exposure.

these results with the pure Mode I case of Figure 5-5 shows similar trends and magnitudes. For the 45° flaw,  $K_I$  is not zero but is very small--less than 1 ksi in<sup>1/2</sup> for the flaw lengths and thermal loads shown in Figure 5-6.

#### EFFECT OF AERODYNAMIC COOLING

In the previous calculations, the flawed panel was assumed stationary so that the surface heat transfer coefficient ( $h$ ) was input as zero (no forced or natural convection). If the panel was moving or if air was being moved over a stationary plate at the given velocity, then the stresses in the panel would decrease because surface cooling would reduce metal expansion in the irradiated region. Likewise, the stress intensity factor for a given flaw condition would also be reduced.

By repeating the thermal stress analysis with convection cooling, the resulting stress intensity factor for a flux of 100 W/cm<sup>2</sup> is given in Figure 5-7. In the thermal analysis, the heat transfer coefficient was estimated from the case of uniform air flow over a flat plate assuming a turbulent boundary layer. At a free stream velocity of 1,100 ft/s (Mach 1), the heat transfer coefficient was computed to be 115 BTU/hr-ft<sup>2</sup>-°F. In Figure 5-7, the ratio of  $K$  to the  $K$  level computed for zero velocity ( $h = 0$ ) is shown as a function of velocities up to Mach 1. For irradiation exposure of 1 second, the reduction in  $K$  is approximately 4 percent at Mach 1. These reduction ratios are approximately the same for all flaw lengths due to the short exposure time. After 4 seconds, however,  $K$  is reduced more with a greater reduction observed for longer flaws ( $a = 1$  inch) than shorter flaws ( $a = 0.25$  inch) as shown in Figure 5-6. The maximum difference between  $K$  for stationary plate to  $K$  in a plate moving at Mach 1 is about 10 percent for the conditions depicted in Figure 5-6. It is expected that the benefits of aerodynamic cooling will become more significant for longer exposures and higher fluxes where temperatures closer to melting could occur. Clearly, the maximum excursion in  $K$  would be limited by the presence of surface cooling for the case of a single laser pulse since the total heat absorbed would be reduced by convection as opposed to just heat conduction alone.

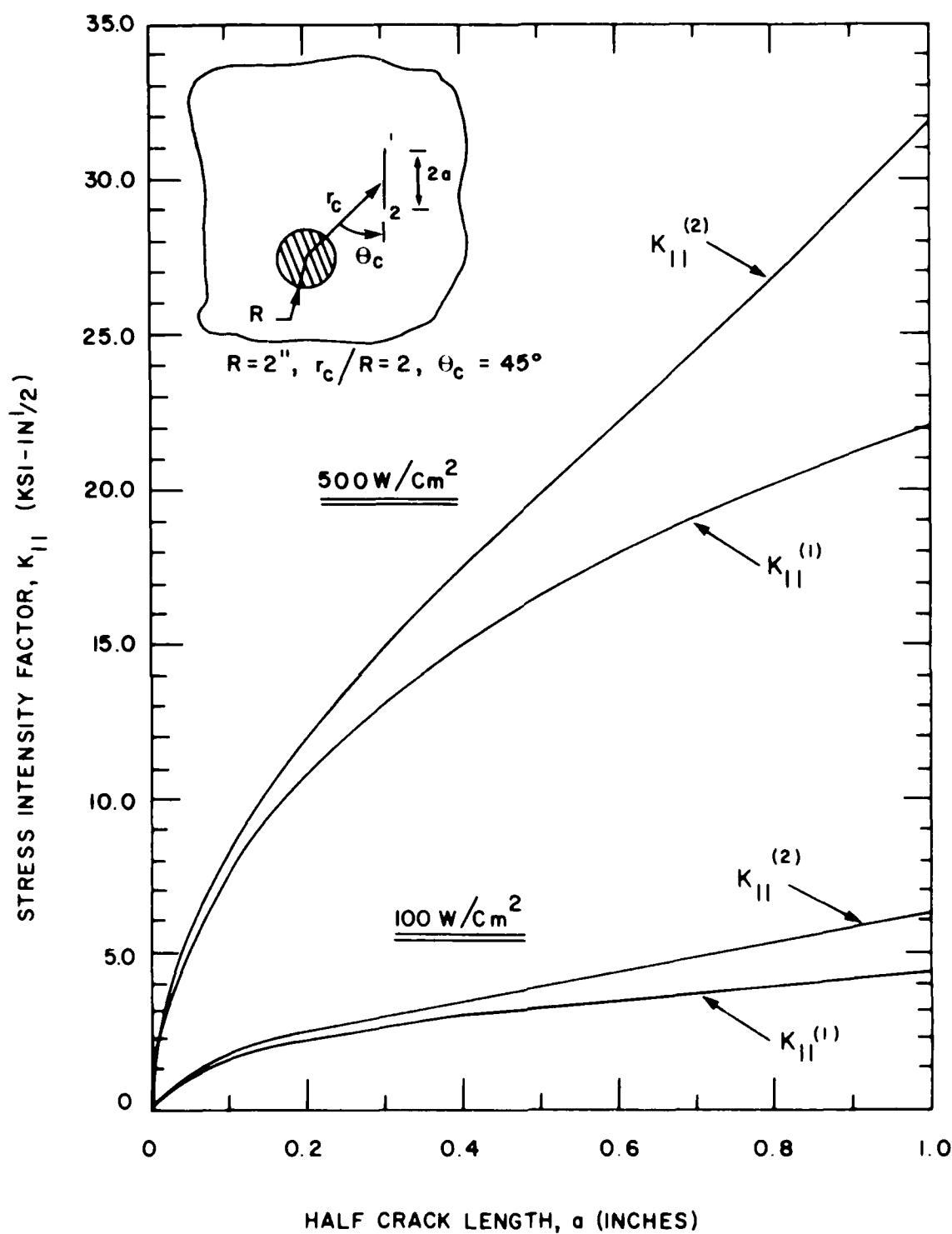


Figure 5-6 - Mode II Stress Intensity Factor for Two Laser Flux Cases After 2 Seconds of Exposure  
(Note:  $K_I \leq 1$  ksi in<sup>1/2</sup> for the Above 45° Crack).

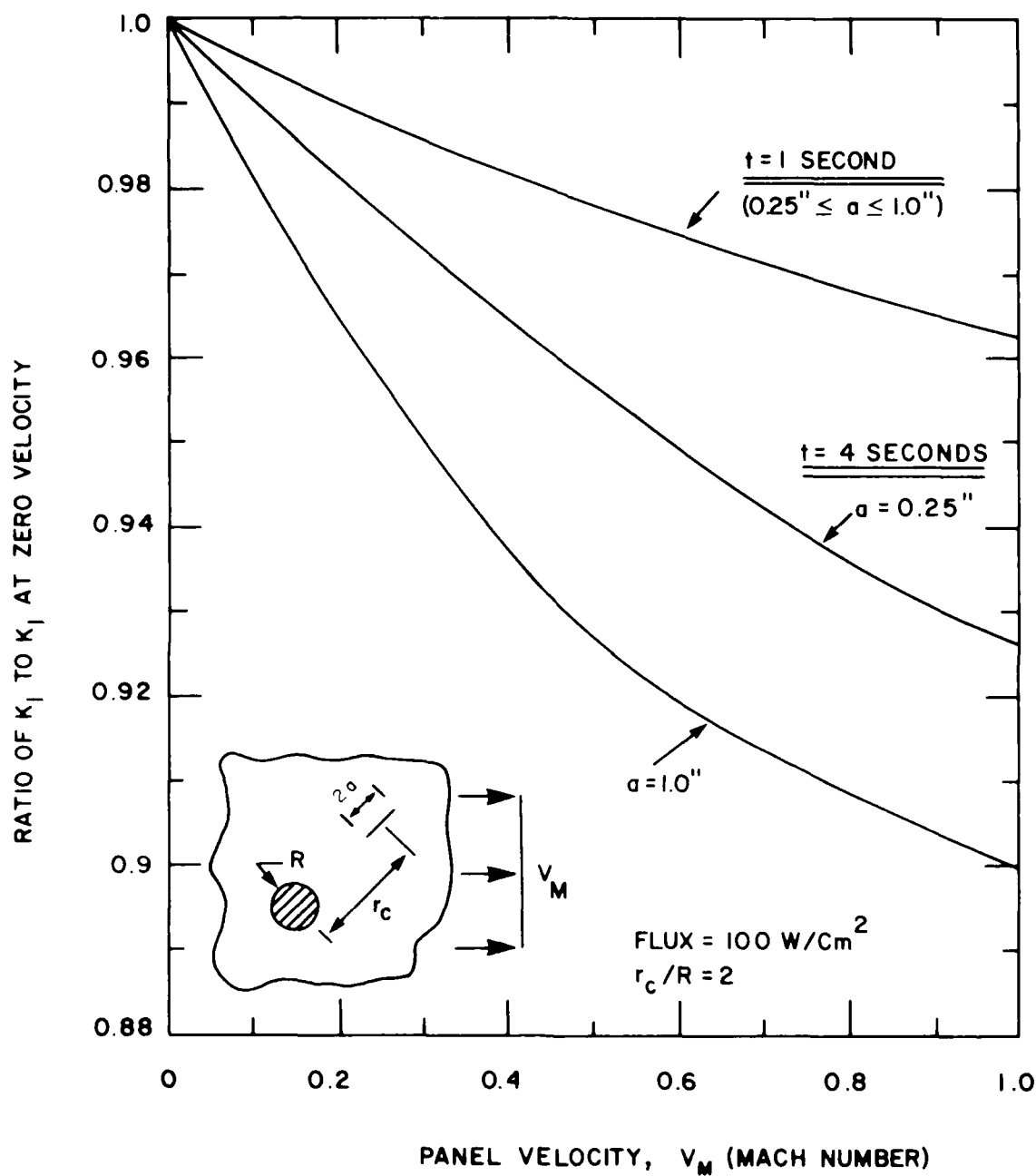


Figure 5-7 - Effect of Aerodynamic Cooling on Stress Intensity Factor.

## Section 6

### AERODYNAMIC HEATING OF A PLANE SURFACE

#### PROBLEM PARAMETERS

A second problem involving the surface heating of a finite thick plate was solved in similar fashion to the laser beam problem. In this example, the edge cracked plate model was used to investigate the effect through thickness temperature gradients have on a two-dimensional surface flow. The thermal model illustrated in Figure 4-3 was used to solve for temperatures and stresses as a function of time. The plate was assumed to be one material (no cladding) with material properties the same as given in Table 5-1 and with a thickness of 1 inch.

Aerodynamic heating is applied uniformly to one side ( $r = 0$ ) and the flow is located on the other side ( $r = w$ ) where the surface is assumed adiabatic. The surface heat flux was modeled as a traditional convective heating with surface reradiation effects associated with a black body radiator. An equivalent heat transfer coefficient and convective gas temperature were estimated from measurements on metallic specimens subjected to space shuttle reentry conditions (21). Maximum heat fluxes of about  $50 \text{ BTU/ft}^2\text{-sec}$  ( $57 \text{ W/cm}^2$ ) and a surface heat transfer coefficient  $0.008 \times 10^{-3} \text{ lbm/ft}^2\text{-sec}$  based on the enthalpy gradient between the wall and the air. An equivalent  $h$  and  $T$  were established from these data by equating surface heat flux with estimated air temperatures at corresponding free stream test pressures and enthalpies to give:

$$h = 18 \text{ BTU/}(\text{hr-ft}^2\text{°F})$$

(6-1)

$$T_\infty = 10,000\text{°F}$$

It should be noted that the resulting heat rate is approximately an order of magnitude less severe than the laser heating problem analyzed in Section 5.

## STRESS SOLUTIONS

The temperature and stress solution for the plate was solved by the implicit finite difference model. The plate was represented by 21 nodes with a linear spacing of 0.05 inch. A constant time increment of 0.1 second was used in all transient solutions. The temperature change for times up to 30 seconds is shown in Figure 6-1. The initial temperature of the plate was 70°F. At 1 second, the surface temperature was computed to be approximately 130°F, but the temperature at  $x = w$  still remains unelevated. At 30 seconds, the  $\Delta T$  across the plate is approximately 100°F.

The tangential ( $\sigma_z$ ) stress for the transient times of 0.1, 1, and 10 seconds is shown in Figure 6-2. Although the stress variation with distance through the thickness is nonlinear, the basic response of the plate will be to bend like a beam due to the thermal upset at the surface. The through thickness stress is negative and relatively small compared to  $\sigma_z$  and, therefore, it is not plotted. Inspection of the stress distributions to 30 seconds indicates that the maximum stress in the region where the flaw will be postulated ( $x/w = 1$ ) occurs between 7 and 10 seconds. The peak tensile surface stress occurs at 9.4 seconds.

## STRESS INTENSITY FACTORS

Again, the influence function method was used to calculate the Mode I stress intensity factor. The  $K$  variation as a function of time is given in Figure 6-3. As suggested by the stress solutions, the peak stress intensity factor occurs at approximately 9 seconds after heating begins and slowly attenuates with time. Five  $K$  curves are plotted, each corresponding to a different but constant crack penetration ( $a/w = 0.1$  through 0.5). Maximum  $K$  level for each flaw depth is observed to occur at approximately the same point in time with the largest value being  $16.9 \text{ ksi-in}^{1/2}$  for a flaw that is

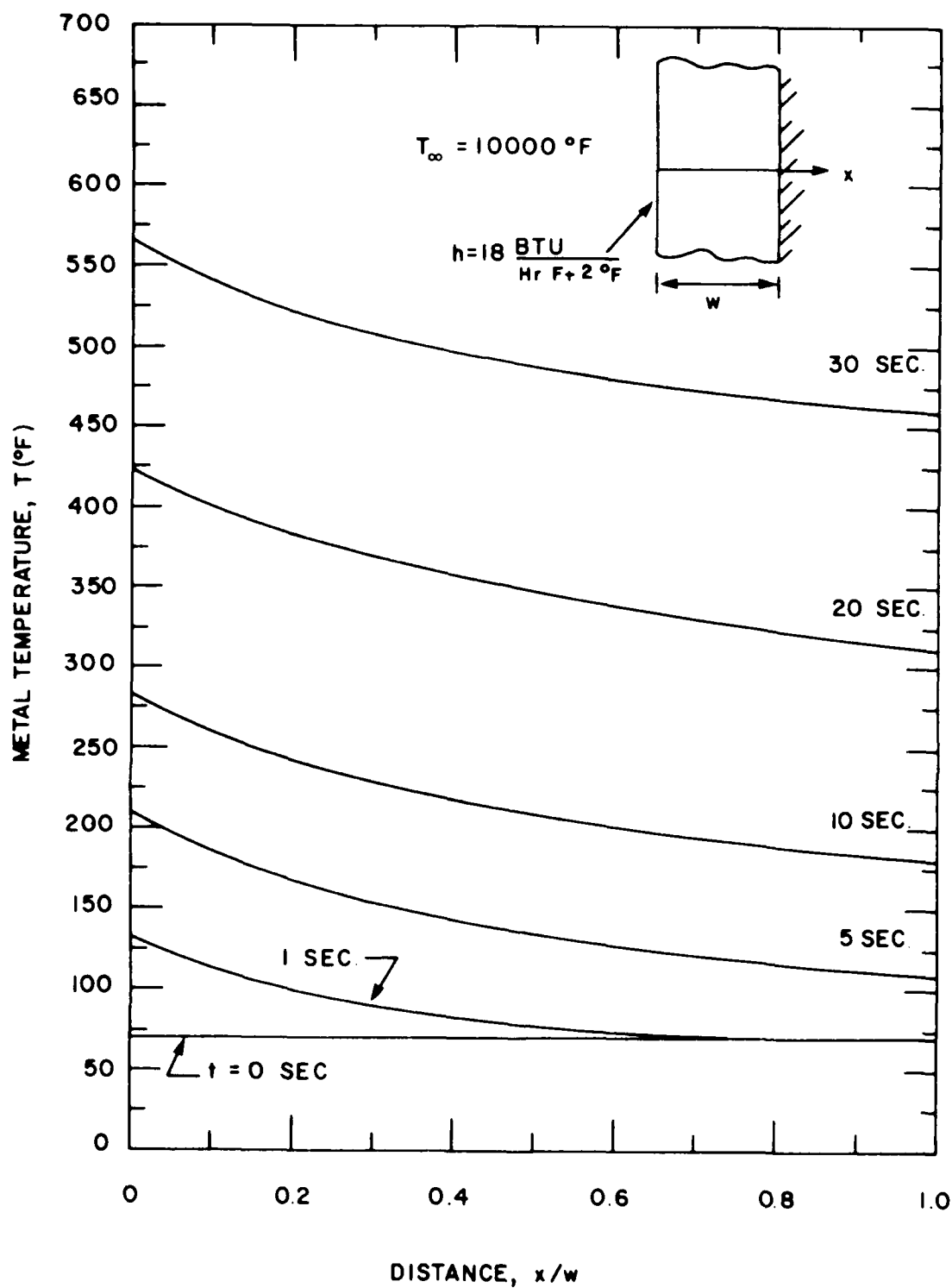


Figure 6-1 - Temperature Response of a Slab Aerodynamically Heated on One Side.

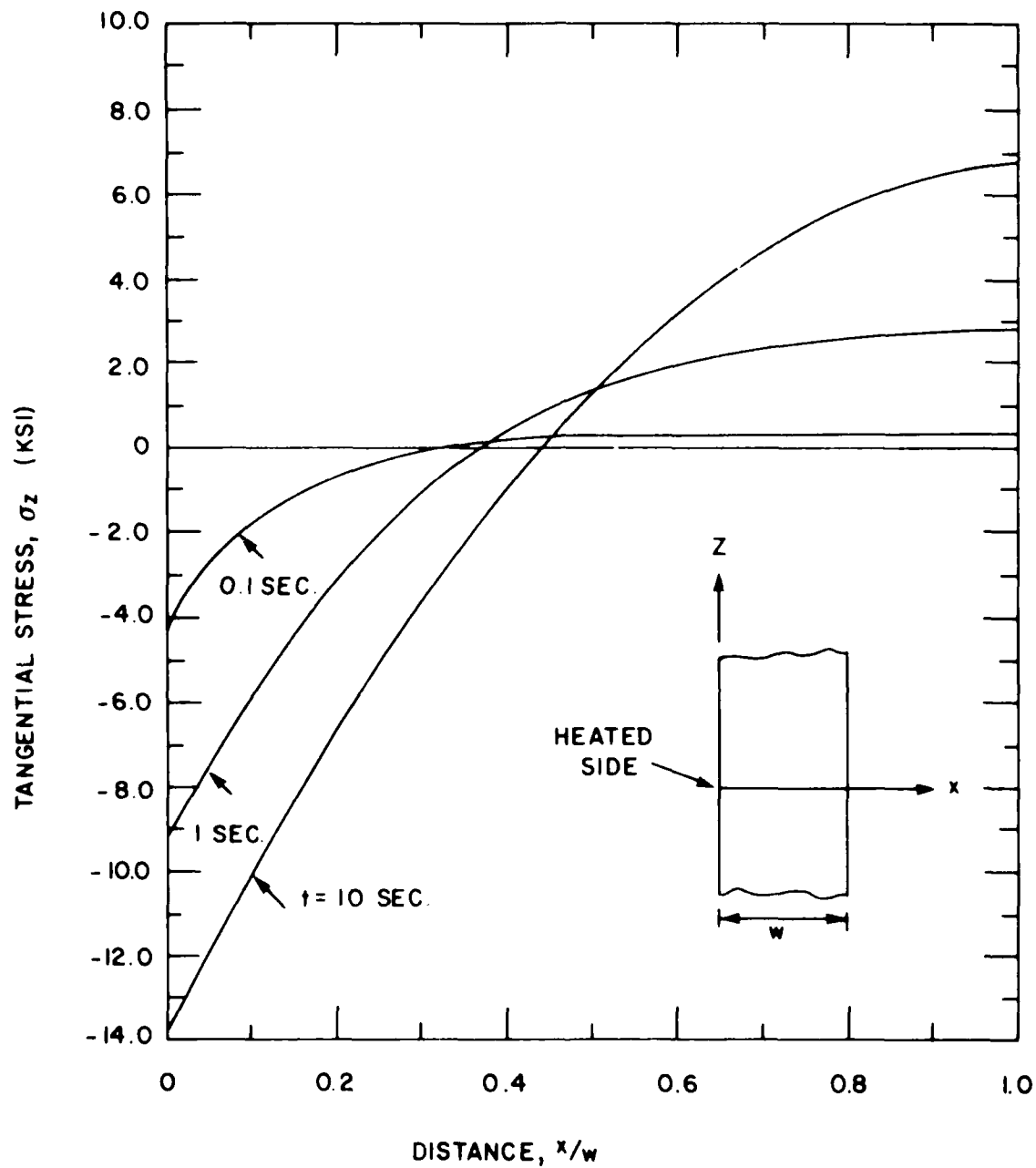


Figure 6-2 - Thermal Stress in a Slab Subjected to Aerodynamic Heating on One Side.

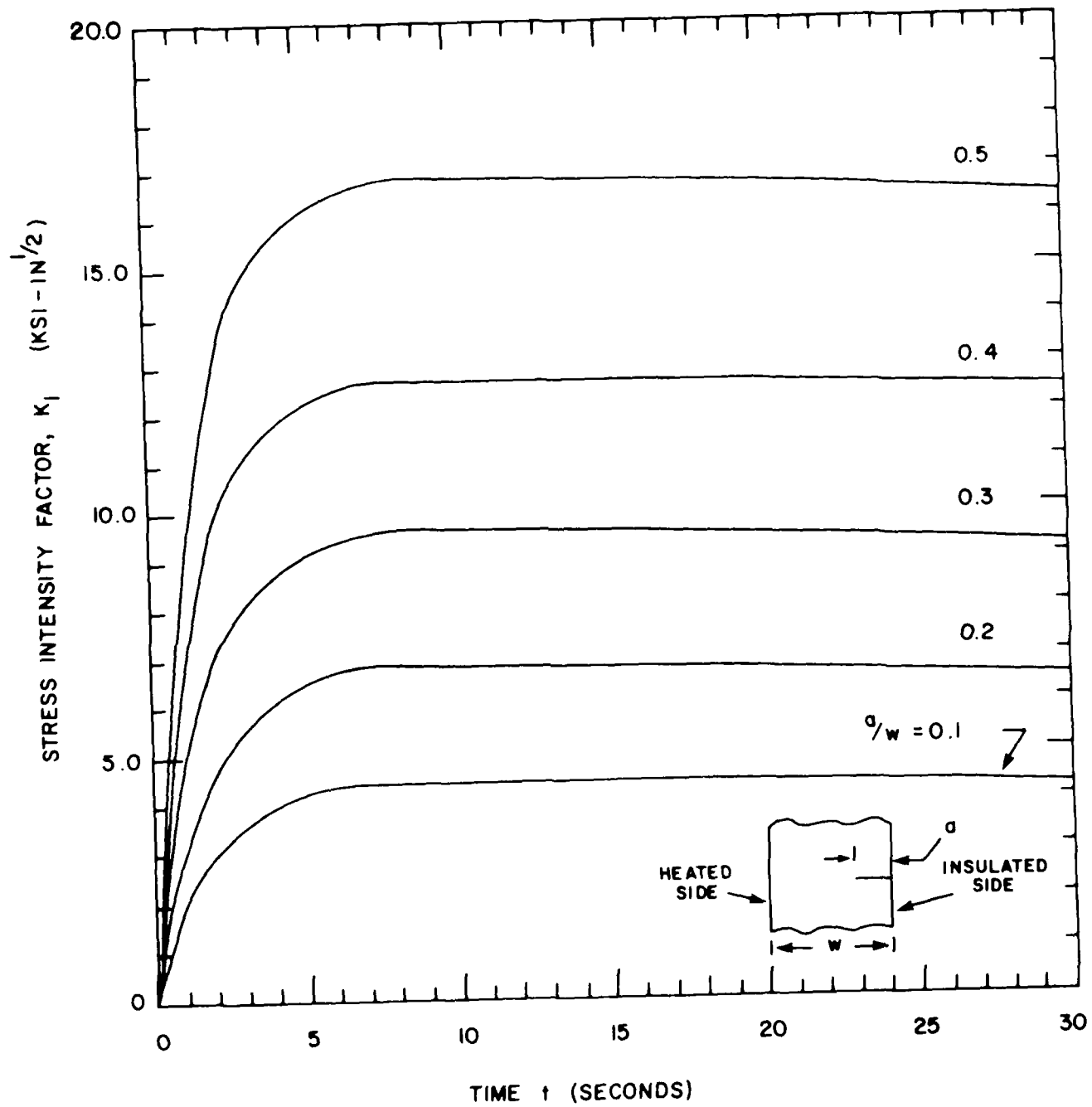


Figure 6-3 - Stress Intensity Factor Variation with Time.

one-half the wall thickness in depth. Because the thermal heating is less severe than the case of laser heating, these calculated stress intensity factors are lower in magnitude.

## Section 7

### COMPUTER HARDWARE AND SOFTWARE REQUIREMENTS

#### INTRODUCTION

The computer programs developed for this investigation were all written in FORTRAN and were executed on an IBM-3081 system located at Stanford University. The FORTRAN language was selected because of its general use in engineering. These programs were written to demonstrate the influence function method and to obtain approximate estimates of execution times for various machines. These computer codes are not considered to be production programs. Further developments will be required before the basic algorithms are suitable for general use. Recommendations for additional capabilities are given in Section 8.

The purpose of this section is to discuss the applicability of these methods for use on desktop computers. Since the major concern here will be accuracy and speed, these two basic characteristics were studied. In addition, a specification for a general purpose program is given.

#### PROBLEM EXECUTION

The problems of laser impingement and aerodynamic heating were solved in two basic steps. First, the thermal stress solution (heat flow and stress analyses) was performed followed by the stress intensity factor solution. Each step was performed by an individual program. The performance of different computers was determined by comparing the execution times of individual microcomputers with the central processing unit (CPU) execution time of the IBM-3081 system.

The microcomputer systems studied were all based on Intel 8088 or 80286 microprocessors in a system architecture similar to IBM-PC/XT and IBM-PC/AT

systems. Because clock speed and the use of a math coprocessor can greatly enhance machine performance, these hardware features were also tested. The coprocessor for the 8088 CPU is the 8087 and the coprocessor used with the 80286 CPU is the 80287. All machines contained and were executed from hard disks.

A summary of individual machine performance was as measured by execution time as shown in Table 7-1. All times listed are in units of seconds. Three problems were solved as shown--a thermal stress solution for laser heating, a thermal stress solution for aerodynamic heating, and a stress intensity factor for an edge cracked plate. Execution times included both CPU time and input/output times associated with the disk. Although the slowest algorithm appears to be the explicit finite difference solution for thermal stress, this problem required many more nodes in the model. Hence, comparison between algorithms should not be made in Table 7-1. It would be expected that the run times for the implicit method would significantly increase with the number of nodes used; however, the stability of the method would allow for larger time increments to be employed.

All execution times displayed by the microcomputers are within the realm of practical application; however, waiting up to 35 minutes for a thermal solution and 20 minutes for corresponding K solution for a 8088 machine without a coprocessor will undoubtedly be annoying to the user. The microcomputers exhibited execution times that ranged from 40 to 1,400 times slower than the IBM-3081 mainframe system. The greatest improvement is observed when a coprocessor is used where a factor of five on speed enhancement was recorded. This is consistent with the math intensive numerical procedure and double precision arithmetic used in the algorithms. A 40 percent speed improvement was observed when clock speed was changed from 4.77 MHz to 8 MHz.

As expected, the 80286 machine was the best performing system with run times less than 1 minute. This class of machines is well suited for the applications intended.

Table 7-1  
SUMMARY OF COMPUTER HARDWARE PROBLEM EXECUTION PERFORMANCE  
(TIMES IN SECONDS)

Solution Algorithm	Problem	IBM-3081 Mainframe <sup>1</sup>	Microcomputer System:		
			8088 CPU 4.77 MHz Coprorocessor	8088 CPU 8.0 MHz Coprorocessor	80286 CPU 8.0 MHz Coprorocessor
Thermal Transient and Stress Solution (Explicit Method) <sup>2</sup>	Laser Heating <sup>2</sup>	1.56	2149	449	312
Thermal Transient and Stress Solution (Implicit Method) <sup>3</sup>	Aerodynamic Heating <sup>3</sup>	0.23	319	67	46
Stress Intensity Factor Solution <sup>4</sup>	Edge Cracked Plate <sup>4</sup>	0.89	1223	242	161
					58
					11
					32

NOTES:

1. The thermal stress solutions were executed with the WATFIV Compiler. The K solutions were executed on FORTRAN Level G Compiler.
2. Transient thermal analysis for 200 nodes for 100 time increments with stresses calculated for 16 time increments.
3. Transient thermal analysis for 21 nodes for 100 time increments with stresses calculated for 16 time increments.
4. Calculation of seven  $\sigma$  versus crack depth distributions each containing 50 discrete values for  $k$ .

The accuracy of microcomputers as compared with the results from the IBM-3081 was excellent. The word length for the 8088 system was determined to be 24 bits for the mantissa. Therefore, the 8088 microcomputer has the same number of significant digits in floating point arithmetic as the mainframe. In fact, the mantissa for single precision arithmetic in the 3081 system ranged between 21 bits to 24 bits depending on the size of the number. This suggests that the microcomputers studied herein, on average, have more precision than the 3081 mainframe.

#### SOFTWARE SPECIFICATION

The software is not organized for production work. Improvements will be required in the area of input/output formats, solution efficiency, and post processing of results. A flowchart showing the general numerical procedure is shown in Figure 7-1. It is proposed that FORTRAN be used wherever possible because of its general use as a scientific programming language. The input to the program will require the greatest development because all well accepted programs are those that are simple to use, to understand, and to modify input files. Programs that can accept both batch input files as well as menu driven input have the greatest flexibility to create new problem input files or change existing or previously created input files. The use of "help files" will greatly improve the speed of solving problems when a users manual is not conveniently available to answer questions.

The solution algorithms can follow the basic structure of the programs. Because these programs were written for solving demonstration problems, their efficiency is not optimum. Additional software will be required to provide for a library of properties for appropriate aircraft structural materials. The properties should cover the temperature range expected for the application of the method. The influence function flaw models should also be organized in a library format for ease of selection and use by the analyst. Recommendations on expanding the capabilities of the present demonstration software are discussed in Section 8.

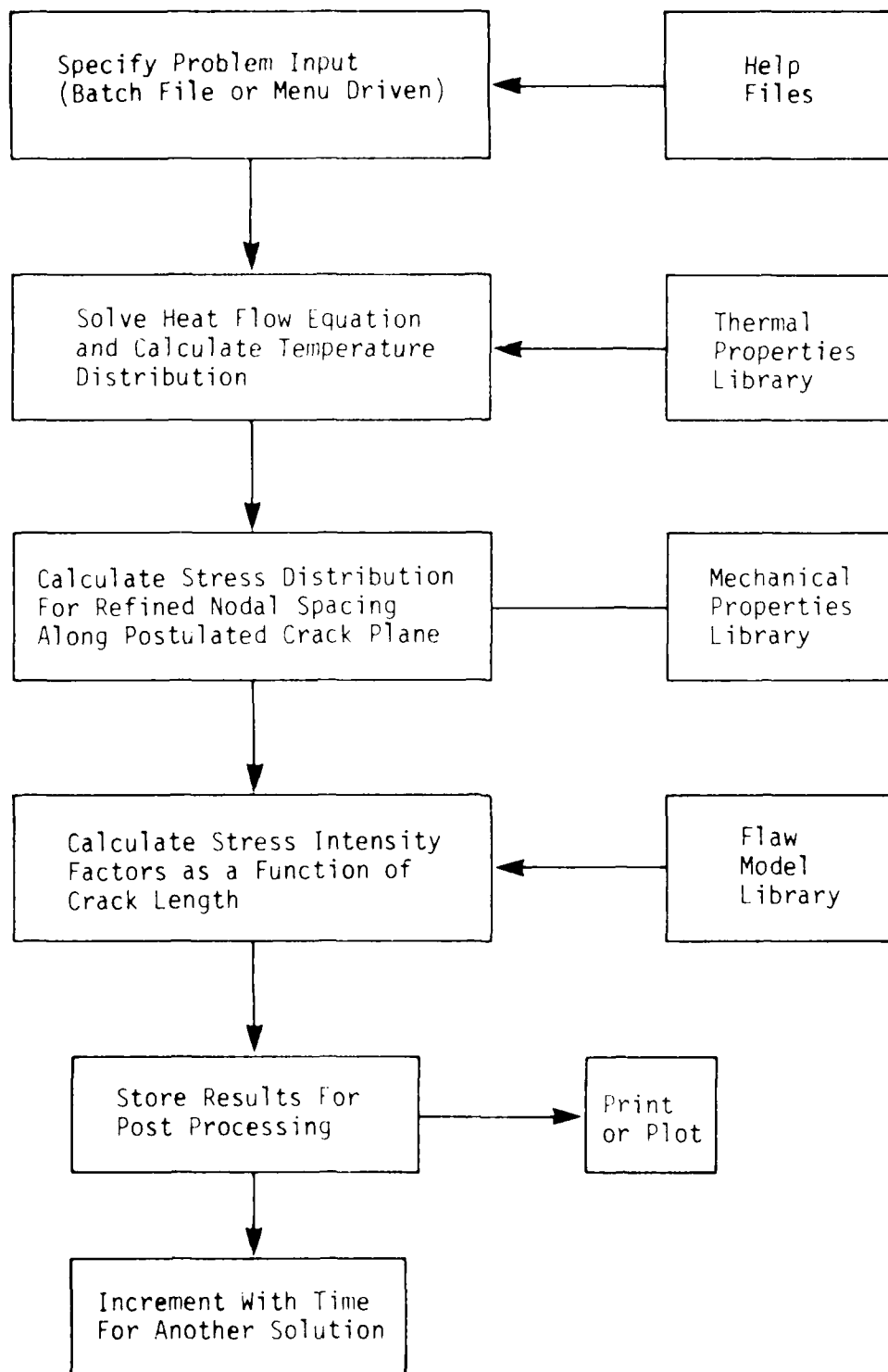


Figure 7-1 - Flowchart Showing General Numerical Procedure.

The processing of output will take the form of either printed summary tables or graphs as selected by the user. Either output format option should have the capability of being displayed on the monitor as well as printed or plotted on a hard copy device. Displaying of results on the computer monitor is very useful in quick problem solving and input iterations, especially if they can be performed in a timeshare environment. Both timeshare and batch environments are easy to implement on a single-user microcomputer system.

## Section 8

### SUMMARY AND CONCLUSIONS

The influence function method is a very powerful technique for calculating stress intensity factors given that the stress state for the structure without the flaw is known. For thermal stress problems, the influence function method is very useful because repetitive K solutions are often required due to time varying stress conditions and multiple flaw orientations of interest. While a knowledge of the stresses along postulated crack planes is required for input to the method, these stress solutions can be solved numerically by algorithms that complement influence function methods in both simplicity and speed. This capability has been demonstrated for two intense heating problems--laser beam impingement and aerodynamic heating. Results from these analyses suggest that stress intensity factors for the thermal conditions assumed can be significant and must be accounted for in structural reliability assessments where severe surface heating is an expected or potential event.

The computer resources required to perform these computations were not significant, and all computations can be performed on currently available desktop microcomputers. Although execution times for microcomputers were very slow compared to an IBM-3081 mainframe system (up to 1,400 times slower depending on microcomputer architecture), problem run times of less than 2 minutes are expected for a 80286-based microcomputer, such as an IBM-PC/AT personal computer. Therefore, the influence function method, including supporting thermal heat flow and stress analysis, can be accommodated by currently available microcomputers that already enjoy wide acceptance and use. Also, the accuracy of the methods did not degrade when executed on the smaller microcomputers. The methods developed herein are, therefore, candidates for use as a desktop design tool as well as an inflight expert system for real time damage assessment.

Because the software developed during this project was for the purpose of demonstrating the methods, the programs are not set up for production problem execution. Additional refinements to the methods are required before the methods can be used on general thermal problems. Specifically, the present programs should be enhanced in the following areas:

- Expand the thermal heat flow and thermal stress numerical procedure to two-dimensional analysis
- Improve the thermal heat flow algorithm for speed and stability; explore more stable methods that are explicit in nature
- Include temperature varying properties and surface phase change (melting, sublimation)
- Expand the number of influence functions to include flaw models for cracks emanating from structural discontinuities, such as holes and stiffener attachments
- Provide for coupling between thermal solution and stress solution when large deflections occur
- Verify accuracy of overall thermal analysis procedure by performing analytical and experimental test problems
- Explore the application of the computer software and hardware developed here to an aircraft onboard expert system
- Prepare user documentation for the method

The laser impingement problem illustrated that local plasticity within the radiation zone and vaporization are possible in extreme cases. At a minimum, these conditions should be checked by the program and the solution procedure modified to account for this. These advanced problems can be handled by the

method provided that the plasticity is contained in the zone and the flaw is well surrounded by an elastic medium. For the case of complete burn through, the situation becomes the problem of a crack in the vicinity of an expanding hole that is being heated on its boundary. Such a case could still be solved by the methods described herein, provided that the proper boundary value problem solution for stress is developed.

In conclusion, the objectives of the project have been achieved. The influence function method is a viable technique for determining stress intensity factors for realistic thermal boundary assumptions. Because of the simple numerical procedure, the method will execute efficiently on small microcomputers.

## REFERENCES

1. Griffiths, C. A., C. I. Chang, and F. R. Stonesifer, "Thermal-Mechanical Response of Tension Panels Under Intense Rapid Heating," Thermal and Applied Fracture Mechanics, Vol. 3 (1985).
2. Patterson, D. M., "Laser Hardened Materials Evaluation and Response Characterization," Air Force Materials Laboratory, Report AFML-TR-78-4098 (December 1979).
3. Bueckner, H. F., "A Novel Principle For the Computation of Stress Intensity Factors," ZAMM, Vol. 50 (1970).
4. Rice, J. R., "Some Remarks on Elastic Crack-Tip Stress Fields," International Journal of Solids Structures, Vol. 8 (1972).
5. Besuner, P. M., "Fracture Mechanics and Residual Fatigue Life Analysis of Complex Stress Fields," Electric Power Research Institute 217-1, Technical Report 2 (July 1975).
6. Cruse, T. A. and P. M. Besuner, "Residual Life Prediction For Surface Cracks In Complex Structural Details," AIAA Journal of Aircraft, Vol. 12, No. 4 (April 1975), Pp. 369-375.
7. Bueckner, H. F., "The Propagation of Cracks and the Energy of Elastic Deformation," Transactions of ASME, Vol. 80E (1958).
8. Hayes, D. J., "A Practical Application of Bueckner's Formulation For Determining Stress Intensity Factors For Cracked Bodies," International Journal of Fracture Mechanics, Vol. 8 (1972).
9. Irwin, G. R., "Analysis of Stresses and Strains Near the End of a Crack Transversing a Plate," Journal of Applied Mechanics, Vol. 24 (1957).
10. Erdogan, F. "On the Stress Distribution on Plates With Co-Linear Cuts Under Arbitrary Loads," Proceedings of the Fourth U. S. National Congress of Applied Mechanics (1962).
11. Bueckner, H. F., "Weight Functions For the Notched Bar," General Electric Company, Report 69-LS-45 (1969).

12. Tada, H., P. C. Paris, and G. R. Irwin, The Stress Analysis of Cracks Handbook, Del Research Corporation (1973).
13. Naval Research Laboratory, "Response of Materials to Laser Radiation," Report AD-785 010 (July 10, 1974).
14. Vonhosenberg, D. V., Method For the Numerical Solution of Partial Differential Equations, American Elsevier Publishing Company, Inc. (1969), Pp. 22-33 and 113.
15. Timoshenko, S. P. and J. N. Goodier, Theory of Elasticity, Third Edition, McGraw-Hill Book Company (1970).
16. Manson, S. S., Thermal Stress and Low Cycle Fatigue, McGraw-Hill Book Company (1966), Pp. 28-29.
17. McAdams, W. H., Heat Transmission, McGraw-Hill Book Company (1954).
18. American Society of Metals, ASM Metals Handbook, Properties and Selection: Nonferrous Alloys and Pure Metals, Vol. 2, Ninth Edition (1979).
19. Cunningham, S. S., and W. T. Laughlin, "The Surface Absorption of Unpainted Alloys at 10.6 Microns," Air Force Weapons Laboratory, Report AFWL-TR-74-12 (March 1974).
20. Air Force Weapons Laboratory, "Predicting the Average Absorption During Continuous Wave Laser Penetration of Painted Alloy," Report AFWL-TR-77-169 (November 1977).
21. Schaefer, J. W., H. Tong, K. J. Clark, K. E. Suchstand, and G. J. Neuner, "Analytic and Experimental Evaluation of Flowing Air Test Conditions For Selected Metallics In a Shuttle TPS Application," National Aeronautics and Space Administration, Report CR-2531 (August 1975).